Institut für Stahlbau
Lehrstuhl für Stahlbau
und Leichtmetallbau

RWTHAACHEN
UNIVERSITY

The present work was submitted to the Institute of Steel Construction.

Aerodynamic scaling of cylindrical structures through surface roughness modification

Bachelor thesis in the degree of mechanical engineering

presented by

Francisco Javier Bravo Lopez

Matr.-Nr.: 362456

Tutor: Dipl.-Ing. Robert Fontecha

Aachen, 11. Oktober 2016

Table of contents

List of Notations

A   Projected area

CD Drag coefficient

Cf Skin friction coefficient

CP Pressure coefficient

D   Diameter of cylinder

FD Drag force

k   Roughness

L   Length of cylinder

P   Gauge pressure

P   Surface pressure

p   Barometric pressure

Pa Absolute pressure

$p0$ Static pressure

µ   Dynamic viscosity

ϱ   Density

$P0$ Total pressure

Re Reynolds Number

$\Psi_{\lambda\alpha}$ Is the end-effect factor

$C_{p,0}$ External pressure coefficient without free-end flow

α_A Is the position of the flow separation

v   Kinematic viscosity of the air (v 15E-06 m2/s)

$V(Z_e)$ Peak wind velocity defined at height z_e

$P0$ Total pressure

Re Reynolds Number

Θ   Angle of incidence in degree

List of figures

ANNEXE A

ANNEXE B

1   Introduction

The study of the performance of bodies in moving (fluids?) is called aerodynamics. The resistance of a body as it moves through a fluid is of huge importance in this field. Drag force, as this resistance is called, affects fuel consumption, range and speed.

The flow around a circular cylinder and the drag force on it have been studied for a long time, as many researchers have studied the effect of surface roughness on cylinders in the past.
Bearman and Harvey (1993) studied the effect of the dimpled at the cylinder surface while roughness on a cylinder was studied by Szechenyi (1975). Both of these studies showed that the pressure distribution around the cylinder could be altered through the addition of a roughness pattern.
The impact of roughness strips and engineered grooves on circular cylinders were investigated by Nakamura and Tomonari (1982) and Kimura and Tsutuhara (1991), respectively. While Nakamura and Tomonari noted that super-critical flows could only be obtained by roughness strips and not roughness patterns, Szechenyi concluded that the outlook was favourable for finding a Surface roughness pattern that could simulate super-critical *Re* at sub-critical *Re*. The study by Kimura and Tsutuhara added that the orientation of the groove with respect to wind direction was critical in predicting the flow around the cylinder.
It is not practical to consider that aerodynamic trips for the model testing of structures will produce varying flows when the model is rotated, such as grooves and strips.

1.1 Motivation

A lot of difficulties are found when trying to simulate super critical *Re* flow effects over cylinder surfaces at relatively low wind speeds in a boundary layer wind tunnel. Simulating the effects of full scale winds over cylinder surfaces on scale models is made difficult due to the contrast in *Re* between the model scale and full scale structures.

The influence of the Reynolds number on a round model is relevant for wind-tunnel tests; it dictates the laminar boundary layer separation point. Normally, the kinematic viscosity ν is the same in the full scale and during the wind tunnel test. If the wind force acts on a 150 m high and 6 m wide tower, the transformation of scale in the wind tunnel a geometrical scale of λ_L= 1:300 and a reference wind speed inside the wind tunnel of V ≈12.5 m/s, the obtained value is about $Re_{wind\ tunnel}$≈ $1.6*10^4$. Comparing this value with the full scale situation, where at 150 m height a wind speed of 39 m/s is calculated, the Reynolds number increased up to $Re_{full\ scale}$≈ $1.6*10^7$.

This huge difference between both Reynolds can be solved if the blower of the wind tunnel produces a wind speed of 10,000 m/s, which is practically impossible. So, it should be accepted that the Reynolds model law cannot be fulfilled inside a wind tunnel due to the scale effects. Therefore, the only practical solution is to simulate flow features which imitate the turbulent boundary layer at high Reynolds numbers by adding roughness on model's surface. That way, super critical regime conditions can be simulated.
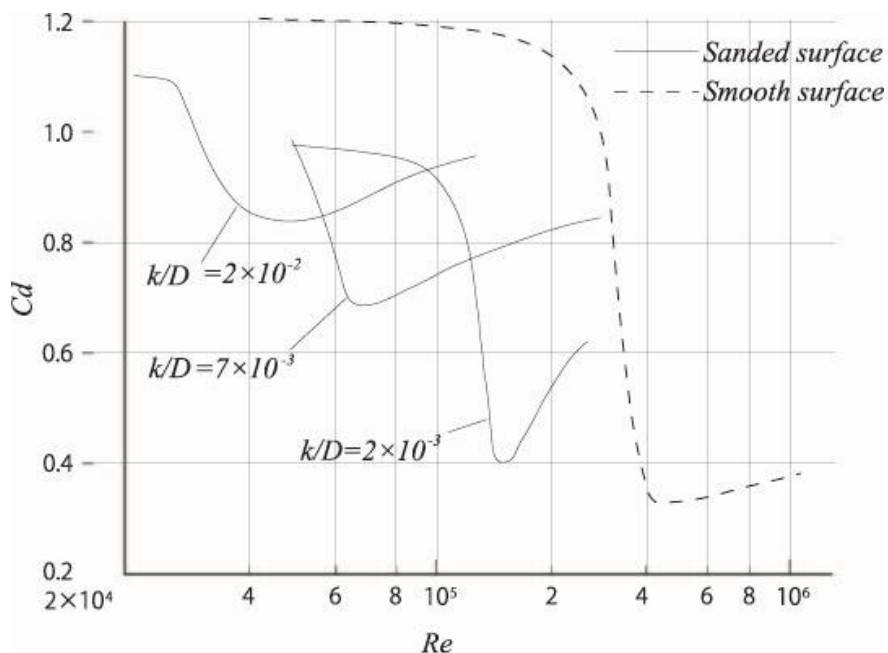
Figure 1.1 Cd depending on the roughness surface

1.2 Approach

This study attempts to control the flow as well as the separation point around a circular cylinder through the implementation of artificial surface roughness across the exterior of the cylinder. In order to do that, roughness indented patterns and several roughnesses with sandpaper will be tested at the circular cylinders' surface, which were subjected to wind laminar flows in a BLWT. Measurements of the pressure distribution across the façade will be also obtained over the Re range of $7x10^3$ to $6x10^4$.

Thus, this study has as a main target to try to simulate super-critical flows conditions with the lowest sub-critical wind velocities so as to apply these results, in case they were optimal, to the project of a real wind tower prototype.

Figure 1.2 Drag coefficient vs Reynolds number

For a comprehensive study, it is necessary to pay attention to some physical characteristics of the flow which should be taken into account during the experiment. Such as the air density p which its value decreases with increasing altitude and depends on the temperature and humidity. The value recommended in the Eurocode is 1,25 kg/m^3.

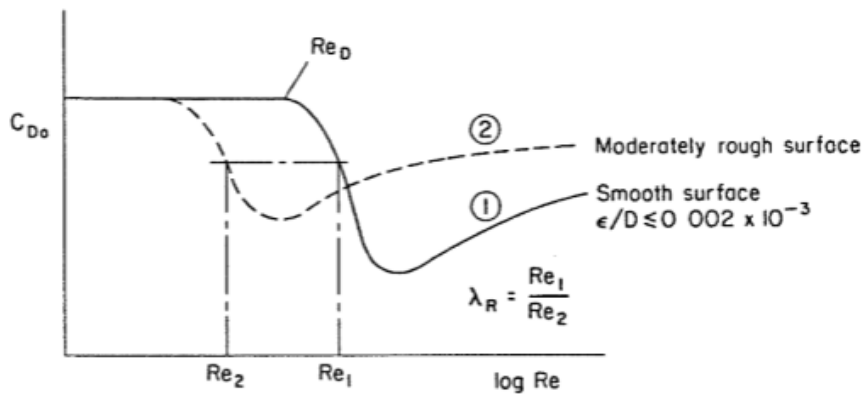## 2   Background

2.1   Reynolds number

A lot of researches had been carried out to predict the variation of drag coefficient depending on the Reynolds number for circular cylinder.

Roshko (1961) showed the measurements on a large circular cylinder in a pressurized wind tunnel for Reynolds numbers ranges from 10^6 to 10^7 and discovered that at high Reynolds number transition the Cd increases from its super critical value to a value of 0.7 at a Reynolds number of about 3.5×10^6. Furthermore, for Re > 3.5 x 10^6, definite vortex shedding occurs, with Strouhal number 0.27.

Achenbach and Heinecke (1981) investigated the vortex shedding phenomena in the range of Reynolds number from 6×10^3 to 5×10^6 as well as the realized the effect of the roughness coefficient of drag for the flow over a circular cylinder.

Shih and Wang et al (1993) observed the effect of the Reynolds number on the distribution of pressure at a low value of Re.

Williamson (1996) has presented comprehensive description of flow phenomena at different range of Reynolds number.

Mittal and Singh (2005) simulated a numerical model to solve the unsteady incompressible two dimensional Navier-Stokes equations in order to studied the instability of shear layer and drag effect in the range of Reynolds number from 10^0 to 10^7 over the flow past a circular cylinder .

Triyogi et al. (2009) used of passive control method to reduce the drag over the I-type small cylinder was carried out, the cutting angle of Θs = 650 is provided as passive control.

M. Sami and M. Salih (2009) used the three turbulence models to compare the computational results for streamline patterns, velocity distributions, vortices contours and drag force coefficients with those of the experiments to examine the effect of mesh size on the numerical simulations.

Larose Guy and Steve (2012) the investigation of reducing drag for a speed skater due to the turbulence effect of wind as presented by them.it was also considered the different range of Reynolds numbers for calculating the drag coefficient as well as the flow separation over circular cylinder results in high dynamic drag force.

Butt and Egbers (2013) presented a discussion about the flow over circular cylinders with the hexagonal patterned surfaces, taking as a reference the range of Reynolds numbers from 3.14×10^4 to 2.77×10^5 into consideration and the well-known characteristics of flows over rough surface.

M. Mallick and A. Kumar (2014) the coefficient of drag can be obtained by two different methods. The Cd obtained by weighing method is more accurate than those obtained from pressure distribution method. It is also known that the drag force increases with increase in diameter of the cylinder. Also, for a cylinder of particular diameter, drag force has been found to increase with increase in air velocity.

The Reynolds number (Re) is a dimensionless quantity which is used to predict similar flow patterns in different fluid flow situations comparing inertial force with viscous force as it can be seen in the formula below.

It is also used to check whether the flow is laminar or turbulent. The Reynolds number is defined by the expression (2.1)

$$Re = \frac{inertial\ forces}{viscous\ forces} = \frac{(mass)(acceleration)}{(dynamic\ viscosity)\left(\frac{velocity}{distance}\right)(area)} = \frac{(\rho L^3)(\frac{v^2}{L})}{\mu(\frac{v}{L})L^2} = \frac{\rho v L}{\mu} = \frac{Lv}{\nu} \qquad (2.1)$$

Where

$\underline{\mu}$ is the dynamic viscosity

v is the maximum velocity

$\underline{v}$ is the kinematic viscosity

$\underline{\rho}$ is the density

L is a liner dimension

2.1.1 Flow separation point

The flow separation point has a huge importance for the drag coefficient Cd of the body, increasing or decreasing its value due to the pressure differences between front and rear parts (Wagner(2010)). Therefore, the drag coefficient Cd is independent of the Reynolds number if the edges are sharp and strongly dependent if the edges are only slightly rounded.

According to Sockel (1984) and Dyrbye u. Hansen (1997), in case of a laminar incident flow on a smooth circular surface, four principal regimes of evolving flow can be identified, depending on the Reynolds number Re:

- Laminar regime: For a low Reynolds number (Re< 200), the flow field remains laminar without any alteration of the flow lines. There is no separation point and there is no pressure drag due to pressure differences between the front and back side of the cylinder. The cylinder experiences only viscous drag due to the air friction.

- Subcritical regime: when the Reynolds number increases (Re up to 10^5), the boundary layer flow is still laminar and separates at about 80° from the stagnation point, as shown in the figure 2.1. Pairs of vortices are formed in the wake. Therefore, a vortex shedding appears and the streamwise length of the vortices increases linearly with the Reynolds number. This is a typical range in case of small diameters D_{ext} or low incident wind velocities V. the drag coefficient in this range of characterized by C_d =1.2.
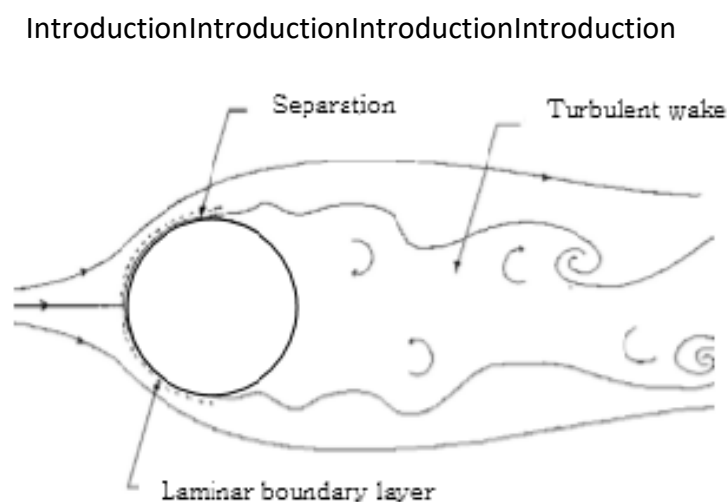
IntroductionIntroductionIntroductionIntroduction

Figure 2.1 Subcritical regime

- Supercritical regime: it appears from the critical Reynolds number $Re_{crit}= 3*10^5$ to $Re= 3*10^6$. The critical Reynolds number can be defined as the value at which the boundary layer changes from laminar to turbulent (Niemann u. Hölscher(1990)).

  As shown in the figure 2.2, a separation point appears on the windward side being it in laminar conditions, but only for a short distance, as the flow then land again on the surface. Behind this, the separation points are located on the leeward side and the turbulent wake becomes much narrower. The drag coefficient C_d can drop to 0.22. Full scale tower normally located in this range.
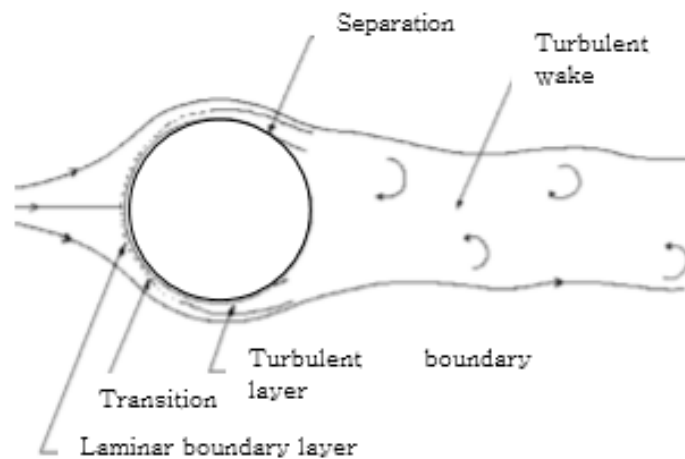

Figure 2.2 Supercritical regime

- Ultracritical regime: also known as transcritical or postcritical regime. Above Re> $3*10^6$, the boundary layer flow at the cylinder surface is fully turbulent and the separation point varies between 100° and 110° from the stagnation point. The Karman vortices reappear and the wake is wider than the supercritical range but narrower than the subcritical regime. The drag coefficient increases again up to a typical range of $0.5 < C_d < 0.9$.

2.2 Eurocode

2.2.1 External pressure coefficients

Pressure coefficients of sections depend upon the Reynolds numbers Re defined by Expression (2.3).
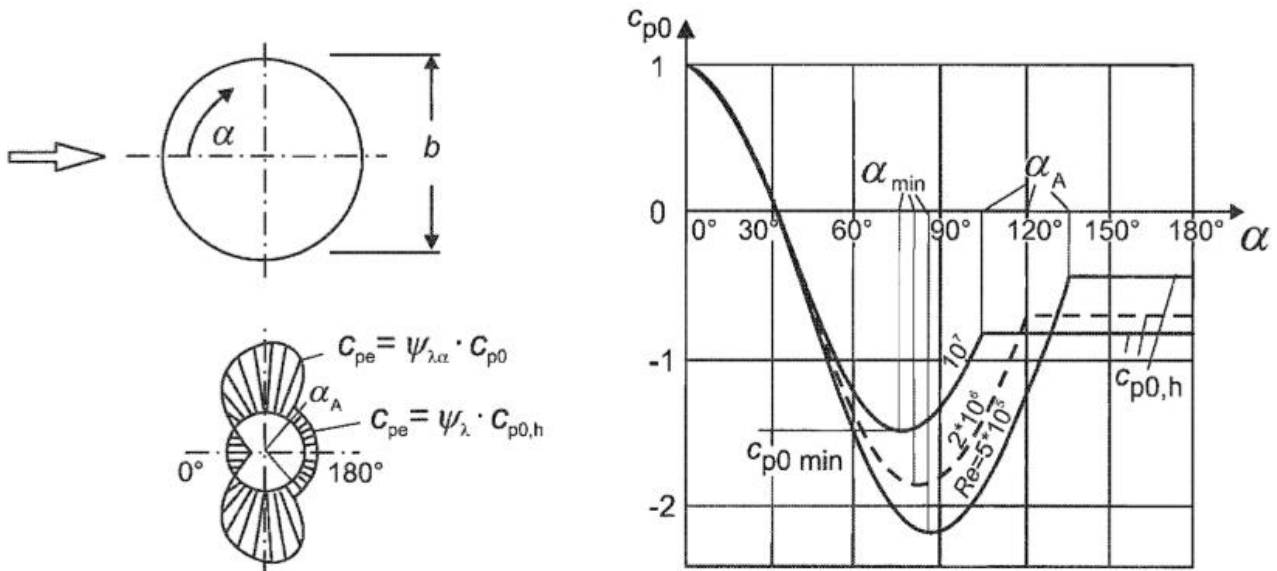
$$Re = \frac{b*v(z_e)}{v}$$ (2.3)

Figure 2.3 External pressure

The external pressure coefficients C_{pe} of circular cylinders should be determined from Expression (2.4).

$$C_{pe=C_{p,0}} * \Psi_{\lambda\alpha}$$ (2.4)

The end-effect factor $\Psi_{\lambda\alpha}$ is given by Expression (2.5).

$\Psi_{\lambda\alpha}=1$ for $0° \leq \alpha \leq \alpha_{min}$

$\Psi_{\lambda\alpha} = \Psi_{\lambda} + (1 - \Psi_{\lambda}) * \cos\left(\frac{\pi}{2}\left(\frac{\alpha-\alpha_{min}}{\alpha_{A-\alpha_{min}}}\right)\right)$ for $\alpha_{min} < \alpha < \alpha_A$ (2.5)

$\Psi_{\lambda\alpha} = \Psi_{\lambda}$ for $\alpha_A \leq \alpha \leq 180°$

The pressure coefficient Cp can be calculated by the expression (2.6)

$$Cp = \frac{P - P_0}{\frac{1}{5}\rho v^2} \qquad (2.6)$$

Where CP = pressure coefficient

P = surface pressure

P0 = static pressure

ρ = air density

V= speed

2.2.2 Force coefficients

The force coefficient Cf for a finite circular cylinder should be determined from Expression (2.7). $\qquad C_{f=C_{f,0}} * \Psi_\lambda \qquad (2.7)$
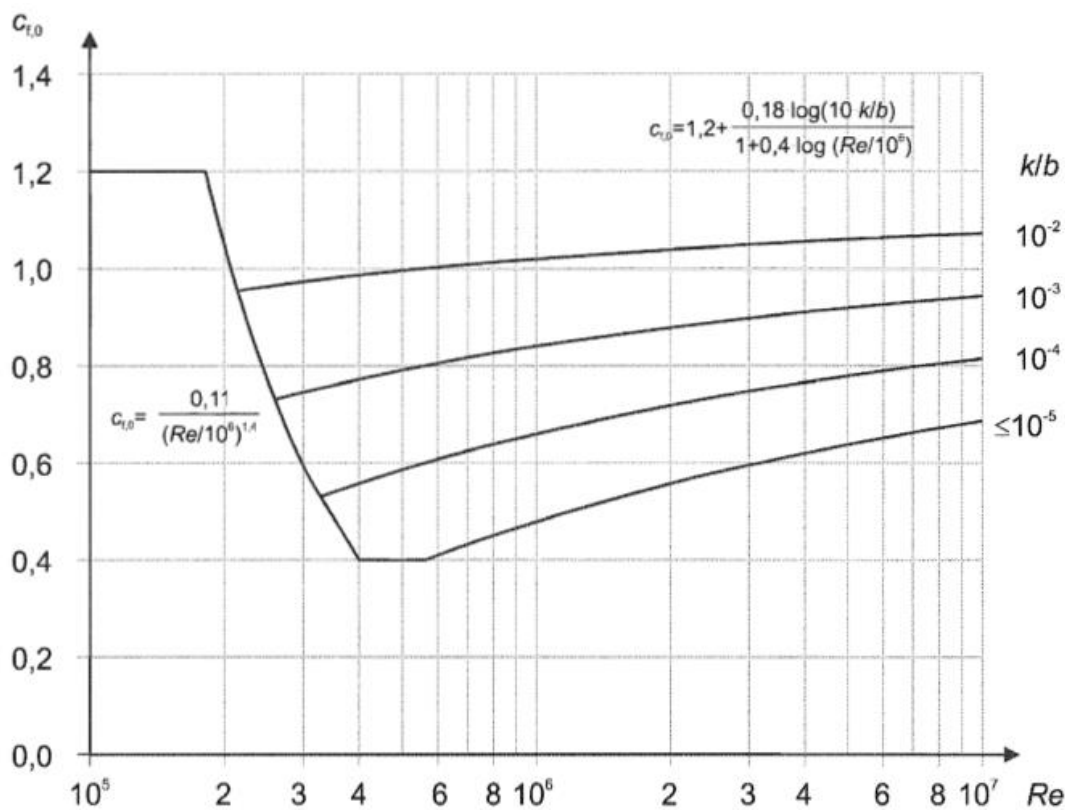

Figure 2.4 Force coefficient

The Figure 2.4 shows the Force coefficient $C_{f,0}$ for a circular cylinder without free-end flow and for different equivalent roughness klb dependig of the Reynolds number.

3 Experimental setup

The first step in the model development stage was to decide what kind of material was going to be used. Plexiglas tubes with 30 mm of external diameter and 26 mm of internal diameter and 750 mm long was finally chosen as a model. Furthermore, 12 holes were drilled along the models circumference at 30° intervals with the purpose of to measure the pressure in the surface of the cylinder as it can be seen in the Figure 3.1.
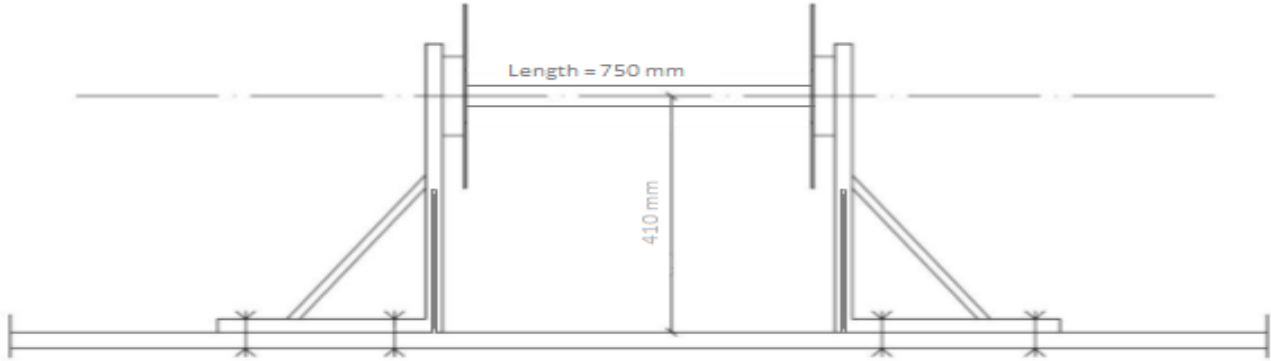

Figure 3.1 structure of the model subjection

Figure 3.2 Rigid construction

A rigid construction was also built to fix the structure to the table, as it can be seen in the Figure 3.2. Thereby, the maximal amount of interferences and vibrations could be avoided.

3.1 Apparatus and equipment used

3.1.1 Numerical control machine

The Pattern of the cylinder surface was made in Inventor. Then, the numerical control machine was used in order to make the roughness indented patterns. A negative form of the cylinder was manufactured with the purpose of fixing the cylinder during the execution of the patterns in order to acquire high accuracies.

Figure 3.3 Numerical control machine

3.1.2 Pressure device

The air come through the tubes fixed in the holes drilled inside the cylinder surface that were connected to the pressure converter where the data was processed and sent to the computer.
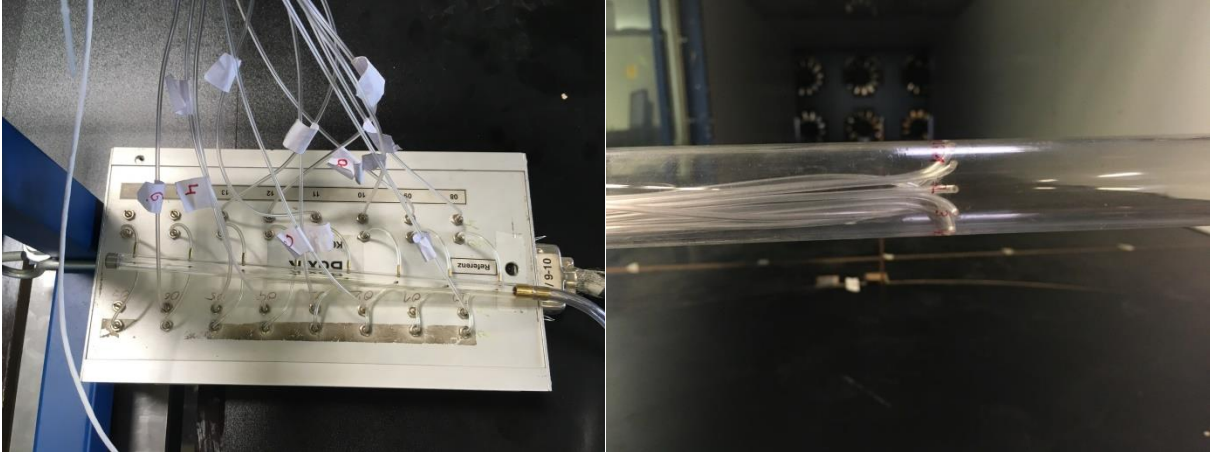

Figure 3.4 Pressure converter

3.1.3 Sensor force devices

The force produced by the wind in the prototype was recollected by two sensors coupled in each extreme of the cylinder (figure 3.5 right), connected through amplifiers (figure 3.5 left) to a computer, where the data was later processed..

Figure 3.5 sensor device

3.2 Wind Tunnel

The wind tunnel of the institute of steel structures works with six motors in a total of 198 KW (6*33 KW) of capacity. The air is compressed through the antechamber in a die and then passed over a run-up track to the rotatory table, which can be fixed if it is necessary. At the exit of the tunnel there is probe which measures the wind speed at the set height.

The dimensions of the section are 9 m long with a diameter of 2,5 m and 1,7 m height. Without disturbing elements, a wind speed of 35 m/s can be achieved.
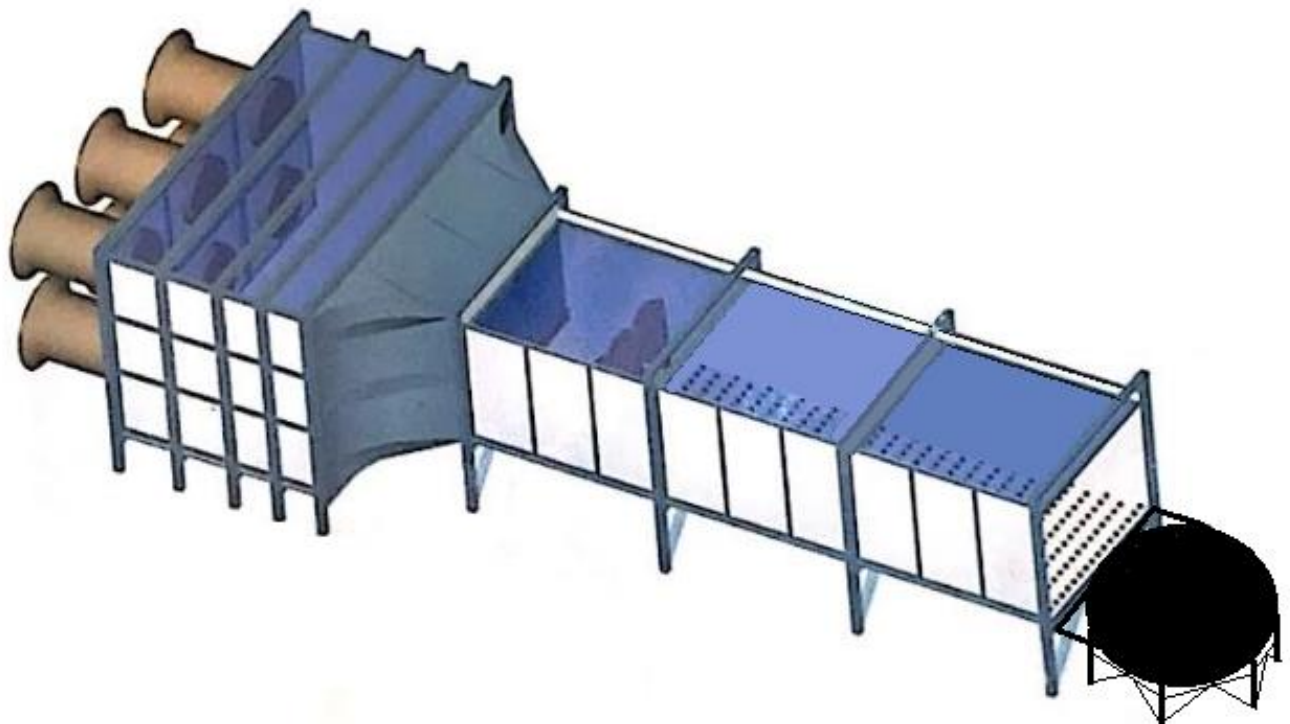

Figure 3.6 wind tunnel

3.3 Cylinder P140, P60, P40

The Plexiglas Cylinder was coated with three different size of sandpaper with the purpose to obtain a wide range of results. However, all of them are designated as a macrogrits.

A double-side tape was used to fix the sandpaper to the cylinder surface. Then, when the sandpaper was totally fixed the holes were drilled and marked, to identify the pressure tubes.

Figure 3.7 P40 model

Figure 3.8 P60 model

Figure 3.9 P140 model

3.4 TATARA prototype

This indented pattern has been taken as a reference from the Tatara Bridge distribution, in the Tetsuo HOJO report "Development of low drag aerodynamically stable cable with indented Processing", which was applied to the cable-stayed in the bridge.

The roughness was described in terms of the depth of the concavities of the pattern, which was designed having the roughness coefficient of 0.01 in the first prototype.

This decision was made based on several researches like the T. Hojo's report which indicate that the 1% of the diameter was the most adequate parameter to reduce the drag coefficient. But in the second pattern of the same distribution a depth of 1 mm was chosen in order to amplify the roughness and maybe get different results.

The cylinder surface was completely machined by the numerical control machine as shown in the Figure 3.11. In consideration of the influence of the flow direction, the pattern was placed at 30 degrees with respect to the axial direction
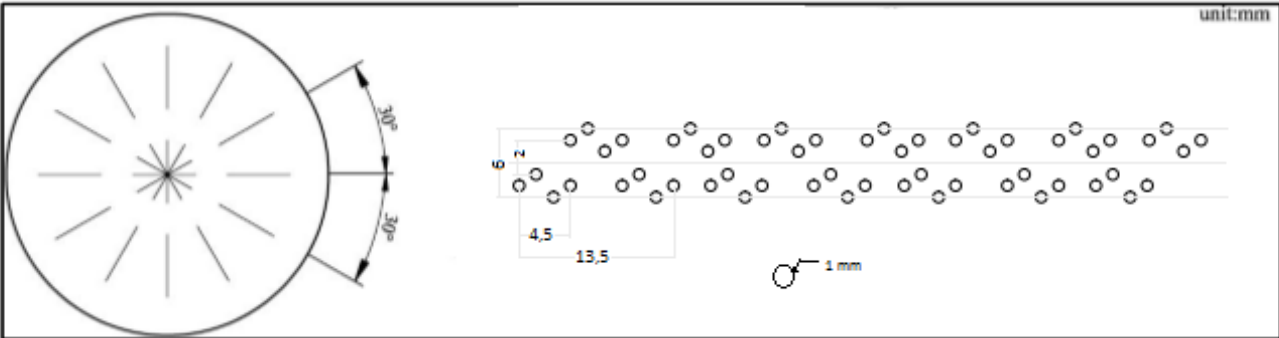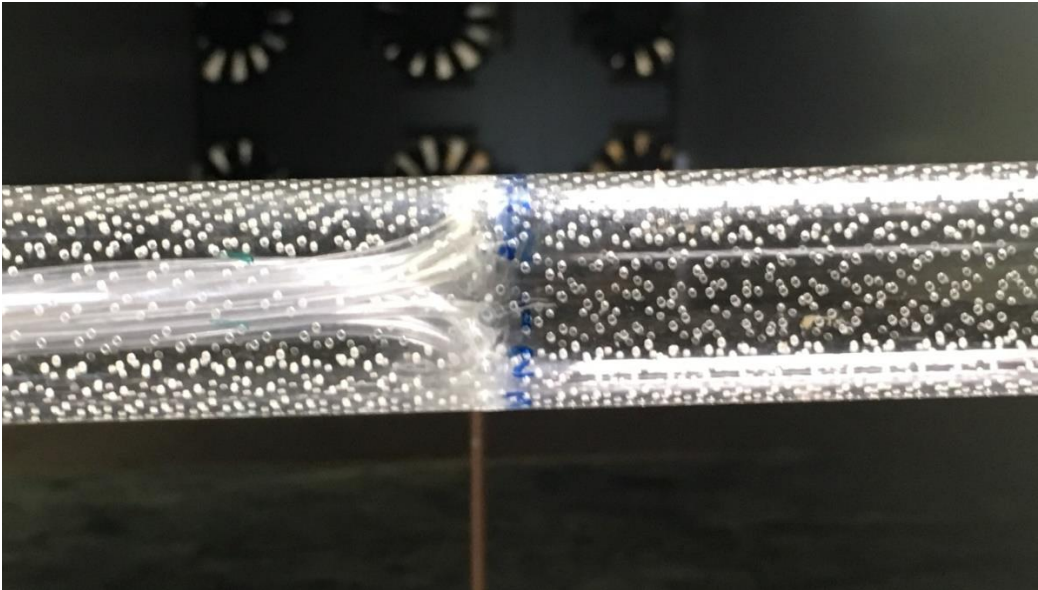

Figure 3.10 Pattern distribution of TATARA Model

Figure 3.11 indented pattern TATARA Model

3.5 Golf Prototype

The indented distribution of P. W. Bearman and J. K. Harvey used in the report "Control of Circular Cylinder Flow by the Use of Dimples" has been taken as a reference to make this pattern. The main idea was to follow the distribution of a Golf ball so as to use the aerodynamic surface to drop the drag coefficient.

The cylinder surface of the Golf prototype was also machined by the numerical control machine as shown in Figure 3.13. In consideration of the influence of the flow direction, the pattern was placed this time at 24 degrees with respect to the axial direction. By rotating the cylinder about its axis, the dimples could be placed in a variety of orientations to the oncoming flow.
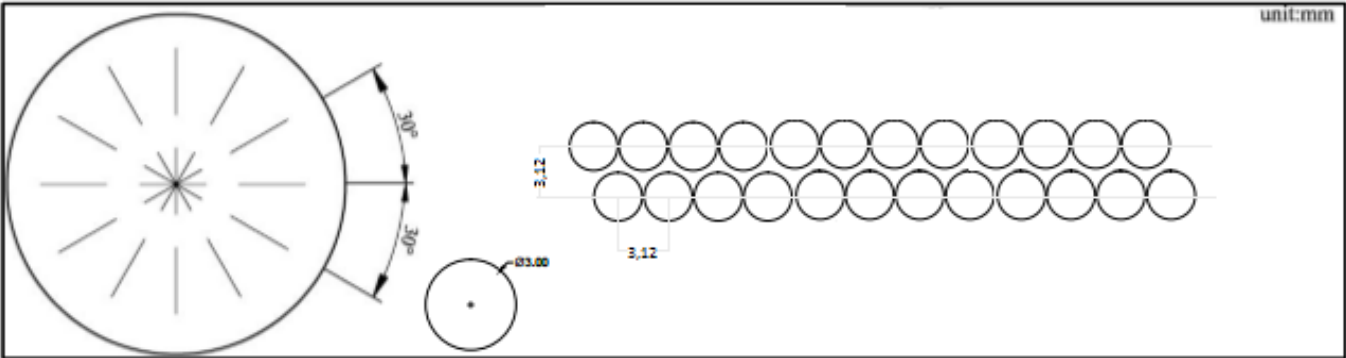

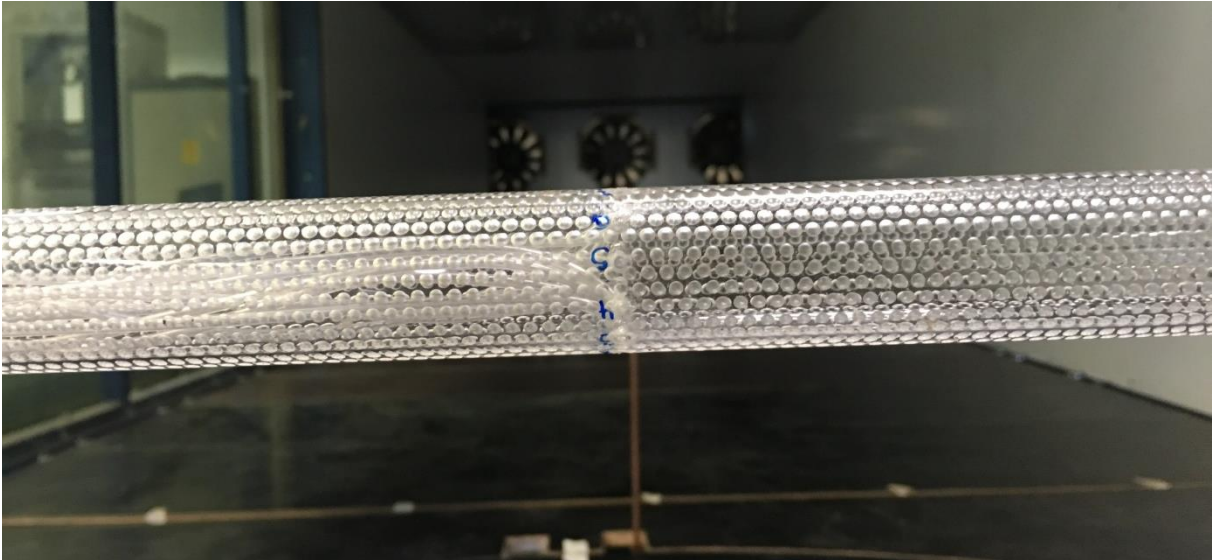**Figure 3.12 Pattern distribution of Golf Model**

Figure 3.13 indented pattern Golf Model

4 Aerodynamic characteristics of a circular cylinder with surface roughness

To investigate the effects of the different surface distributions chosen to control the flow around the cylinder and simulate the conditions of a super critical regime, a wind tunnel test was carried out. In order to clarify the influence of the surface roughness in the drag coefficient, seven kinds of model with different shapes and roughness coefficient were used in the test as shown in the table 4.1.

Model	Diameter D(mm)	Surface roughness k(μm）	Roughness coefficient (k/D)	Remarks
smooth	30	-	-	smooth
P40	30	425	$1,416 \times 10^{-2}$	sandpaper
P60	30	269	$8,96 \times 10^{-3}$	sandpaper
P140	30	115	$3,83 \times 10^{-3}$	sandpaper
golf	30	1000	$3,33 \times 10^{-2}$	Indented pattern
TATARA	30	500	$1,66 \times 10^{-2}$	Indented pattern
TATARA 1mm	30	1000	$3,33 \times 10^{-2}$	Indented pattern

Table 4.1 Dimensions of models

The Table 4.1 shows the measured relative drag coefficients against Reynolds numbers for all the investigated configurations. The measurements were carried out up to a wind speed of 30 m/s with a maximum Reynolds number of 6,00E+04.

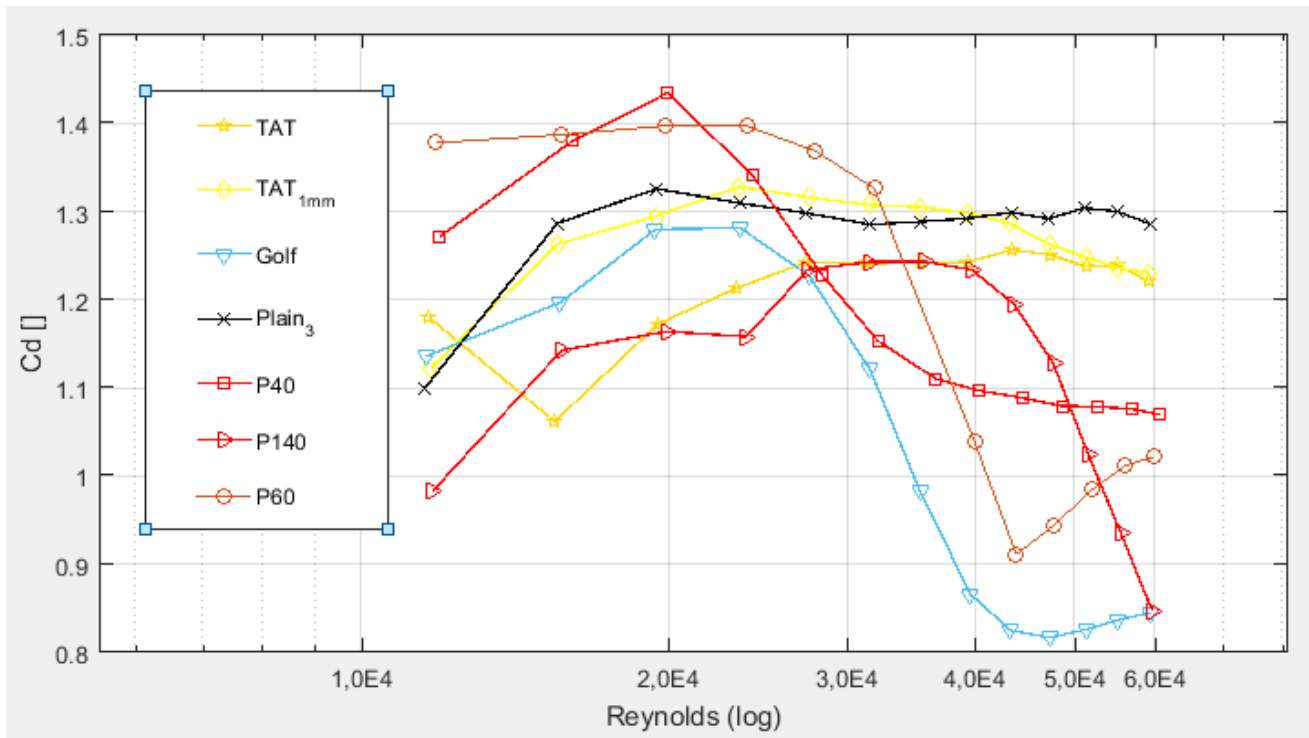**Figure 4.1 Drag coefficient of all the Model**

4.1 Aerodynamic properties of a circular cylinder with sandpaper surface

In this paragraph, the effects of the sandpaper roughness over the flow around the cylinder surface are studied. In order to do that 3 different grit sizes, based on the results of previous studies, have been tested.

Model	Diameter D(mm)	Surface roughness k(μm)	Roughness coefficient (k/D)	Remarks
smooth	30	-		smooth
P40	30	425	$1,416 \times 10^{-2}$	sandpaper
P60	30	269	$8,96 \times 10^{-3}$	sandpaper
P140	30	115	$3,83 \times 10^{-3}$	sandpaper

Table 4.2 Dimensions of sandpaper models

Figure 4.2 shows measured drag coefficient for the three sandpaper prototype and the smooth cylinder. It can be clearly seen that the critical Reynolds number becomes lower as the relative roughness becomes coarser. It was also observed that the larger the surface roughness, the larger became the drag coefficient.

Although the drag coefficient seems to be for all the models a little bit higher than usual, the behaviour of the Cd depended on the roughness coefficient agreed quite well with those reported previously published in this range of relative k/b.

For the model P60, the drag coefficient became 0.9 at the critical Reynolds number of $4.4x10^4$ and 1.03 at a Reynolds number of $6.0x10^4$, equivalent to a wind velocity of about 30m/s. Thus, how it was mentioned above the model P40 as it has a higher roughness coefficient will approach a lower value of critical Reynolds number, 1.44 at a Reynolds number of $2.0x10^4$. Although it shows a different trend from the P60 model, maybe because of the high coarse configuration.

The critical Reynolds number of the model P140 cannot be seen in the Figure 4.2 due to the low range of Reynolds which has been used in this research but the tendency is quite similar to the P60 Prototype.
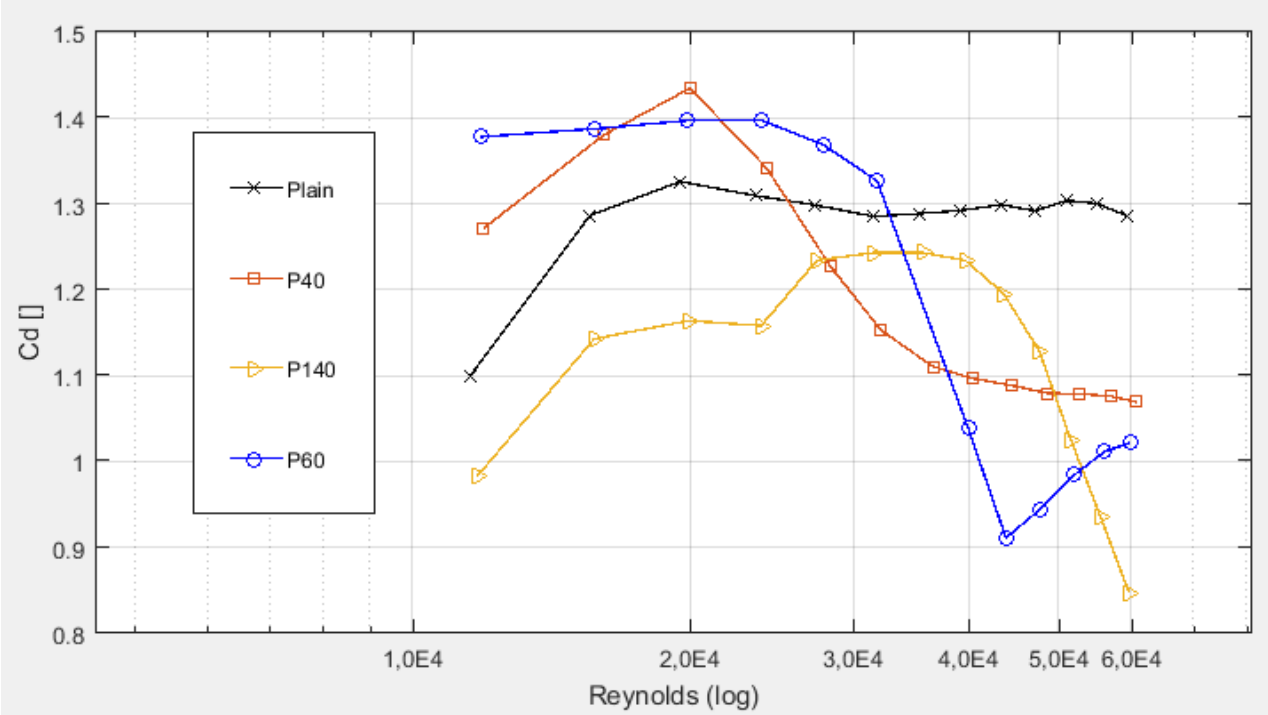

Figure 4.2 Drag coefficient of sandpaper model's

4.2 Aerodynamic properties of a circular cylinder with pattern indented surface

To investigate the effect of the indented pattern over the flow around the cylinder surface 2 different distribution were tested, having roughness coefficient of 0.01 for the TATARA configuration. The Golf as well as the TATARA 1mm distribution was designed with a different configuration. This time 1 mm of depth was chosen as a concept of surface roughness, in order to get more information about the behaviour of the higher roughness coefficient in the drag coefficient.

Model	Diameter D(mm)	Surface roughness k(μm)	Roughness coefficient (k/D)	Remarks
smooth	30	-	-	smooth
Golf	30	1000	$3,33 \times 10^{-2}$	Indented pattern
TATARA	30	500	$1,66 \times 10^{-2}$	Indented pattern
TATARA 1mm	30	1000	$3,33 \times 10^{-2}$	Indented pattern

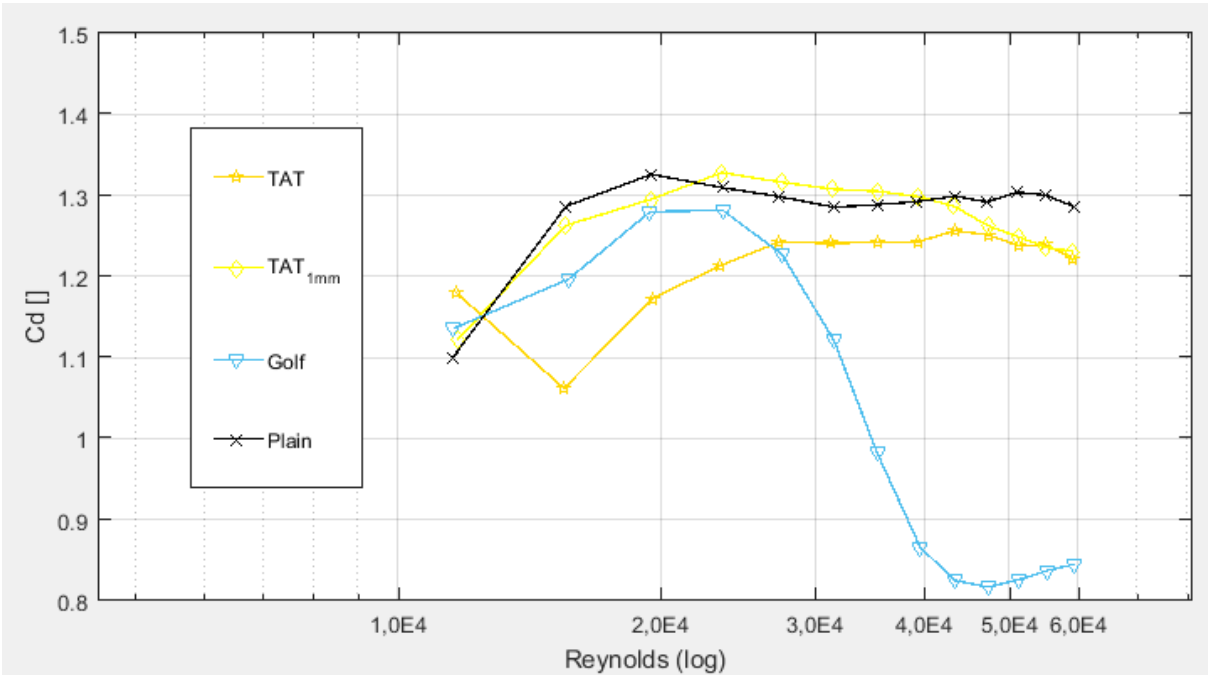**Table 4.3 Dimensions of models**

Figure 4.3 Drag coefficient of indented Model
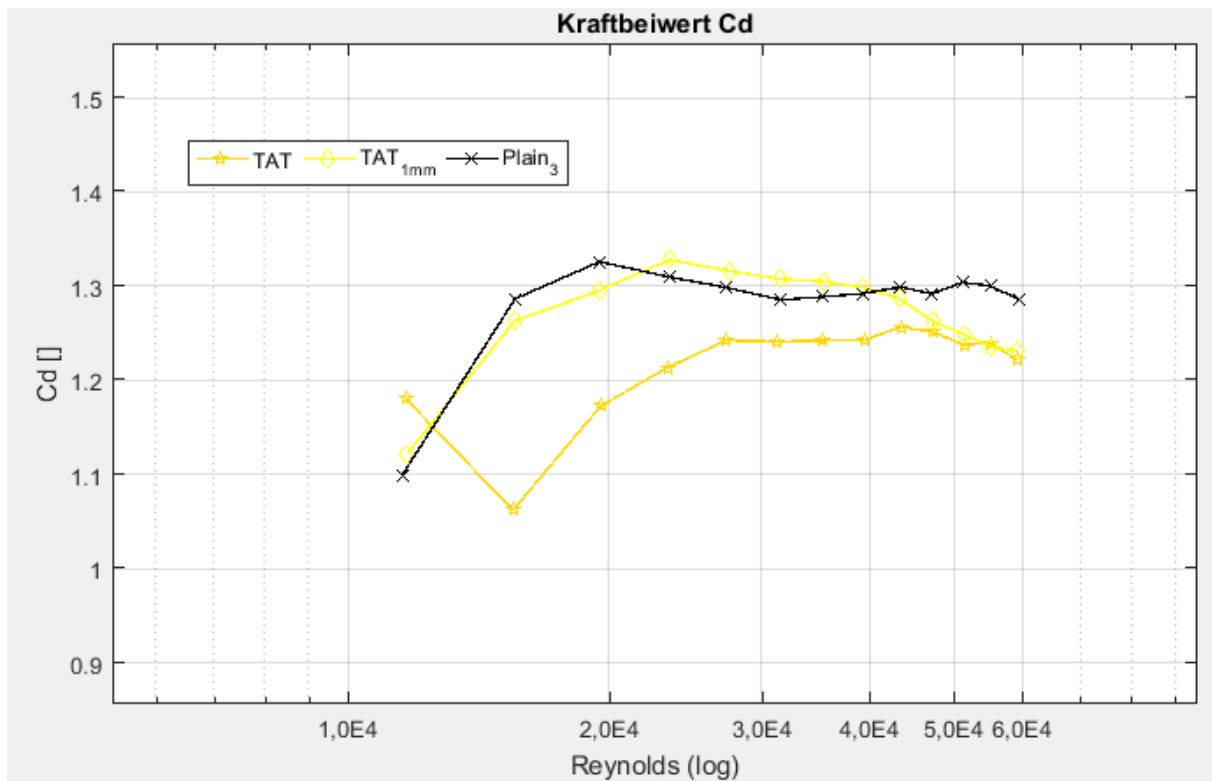
4.2.1 TATARA indented pattern

Figure 4.4 Drag coefficient of TATARA Models

Figure 4.4 shows the drag coefficient of the TATARA and TATARA 1mm model which had the same pattern distribution. However, the drag characteristics were totally different because of the variation in the roughness surface.

The critical Reynolds number of the model with the roughness coefficient about 0.01 (TATARA) becomes 1.07 at a Re = 1.6×10^4. With increasing wind velocity, the drag coefficient has a tendency to increase and rapidly approach the 1.24 where remain almost constant.

The trend of the TATARA 1mm model is quite similar to the Smooth cylinder. This feature is possibly because of the high surface roughness of the TATARA 1mm pattern which acts as a smooth part on the surface. This means that the surface roughness with a partially smooth surface gives the substantial change to the characteristic of the flow of the surface, having a smooth part effect to some degree of the process.

4.2.2 Golf indented pattern

The Figure 4.5 shows the measurements of drag coefficient vs Reynolds number for a dimpled circular cylinder over a range of Re from $1.2x10^{-4}$ to $6.0x10^{-4}$. It is also shown the results for a smooth cylinder with the purpose to compare the effect of both configurations.

The minimum value of drag coefficient for the Golf model as well as the critical Reynolds number occurs at about Re = $4.7x10^{4}$, with a drag coefficient value of 0.81. The highest Reynolds number tested the Cd seems to be approaching to the same value as the smooth cylinder, which remains almost constant to this range of Reynolds in 1.3.

Experimental results of this model had similar characteristics as the dimpled cylinder results shown in the report from P.W. Bearman and J.K.Harvey. Although, Bearman got a range of Cd lower than the Golf model which is normal due to the roughness coefficient from the golf model is higher than the Bearman model.
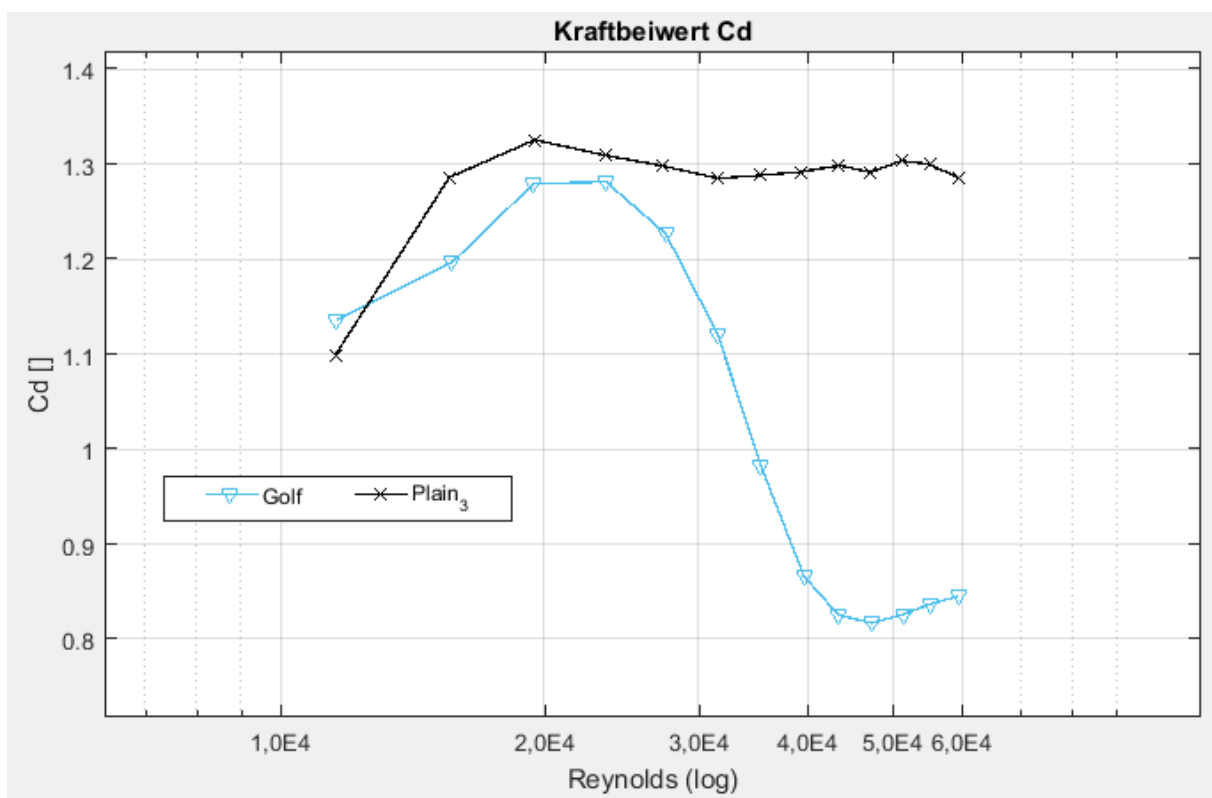

Figure 4.5 Drag coefficient of Golf Model

5 Pressure distribution of a circular cylinder with different surface roughness

The pressure configuration was thought as a tool where it could be seen in which part the separation point at the cylinder surface took place, so as to know whether the conditions of the super critical regime were simulated. The separation point was defined as the point where the Cd curve turned from upward to level.

5.1 P140, P60, P40 surface roughness

Figure 5.5.1 shows measurements of pressure at the cylinder surface. With the P140 model, in the subcritical range, the location of the separation point was about 80° for a Reynolds number of 4.2×10^4.

It can be clearly seen when flow the flow around the cylinder changes from the subcritical regime to the supercritical regime at a Reynolds number of 5.6×10^4. So the separation point, in this case was located at an angle θ of 120°. This means that the P140 model had already reproduced the supercritical conditions at a wind velocity of about 24 m/s.
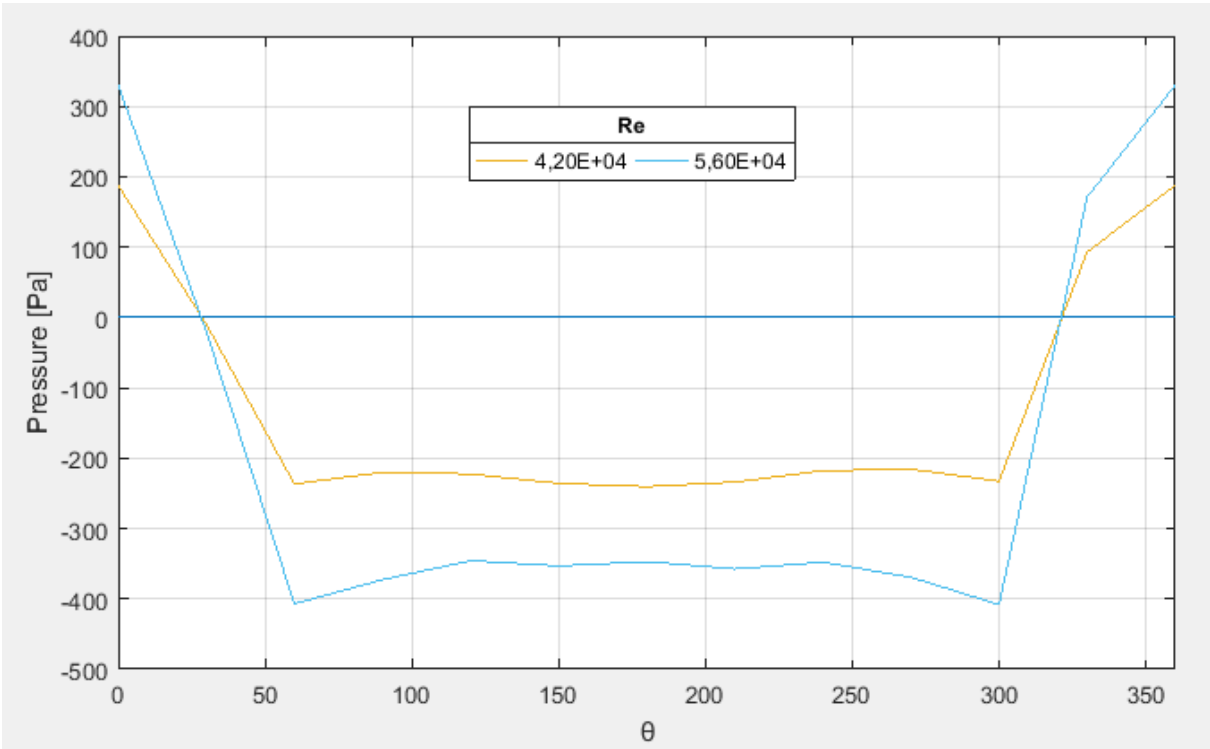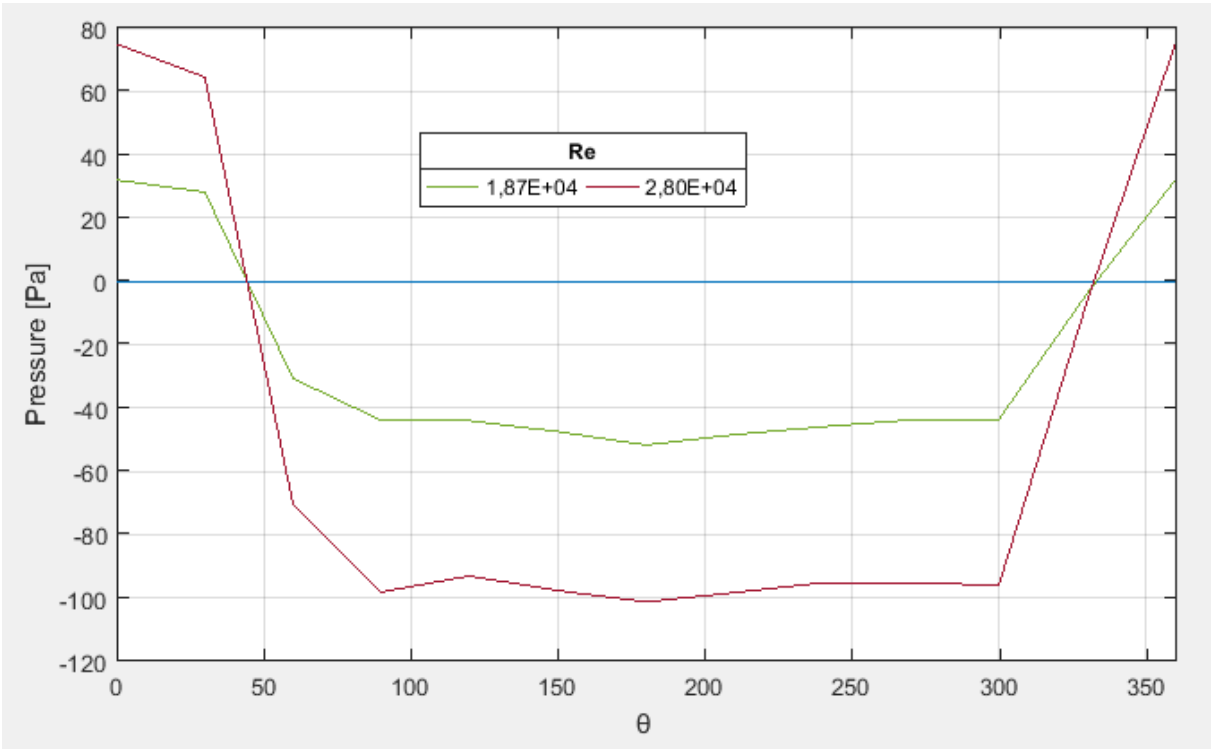

Figure 5.5.1 Pressure distribution of model P140

Figure 5.2 shows the distribution of mean surface pressure around the P60 model at Reynolds number of 2,8x10^4 and 4,2x10^4. With the P60 model, in the subcritical range, the location of the separation point was about 80° for a Reynolds number of 2.8x10^4, and the pressure on the rear surface remained almost constant, taking place the flow separation at the rear surface.

However, in the supercritical regimen at a Reynolds number of 4,2x10^4, the separation point moved backward an angle of 120°, and the static pressure on the rear surface came back to its previous position due to the turbulent at the surface. So, this proves that the P60 model was already in the supercritical regime as can also be checked in the Figure 5.2.
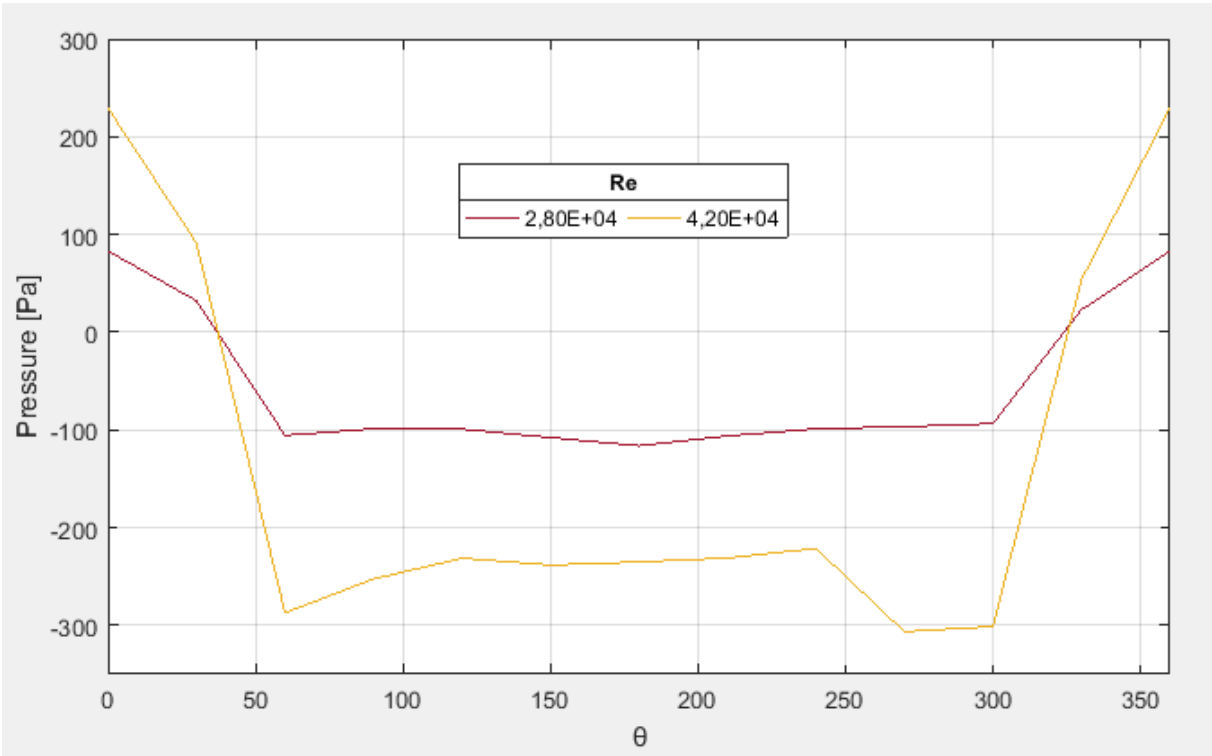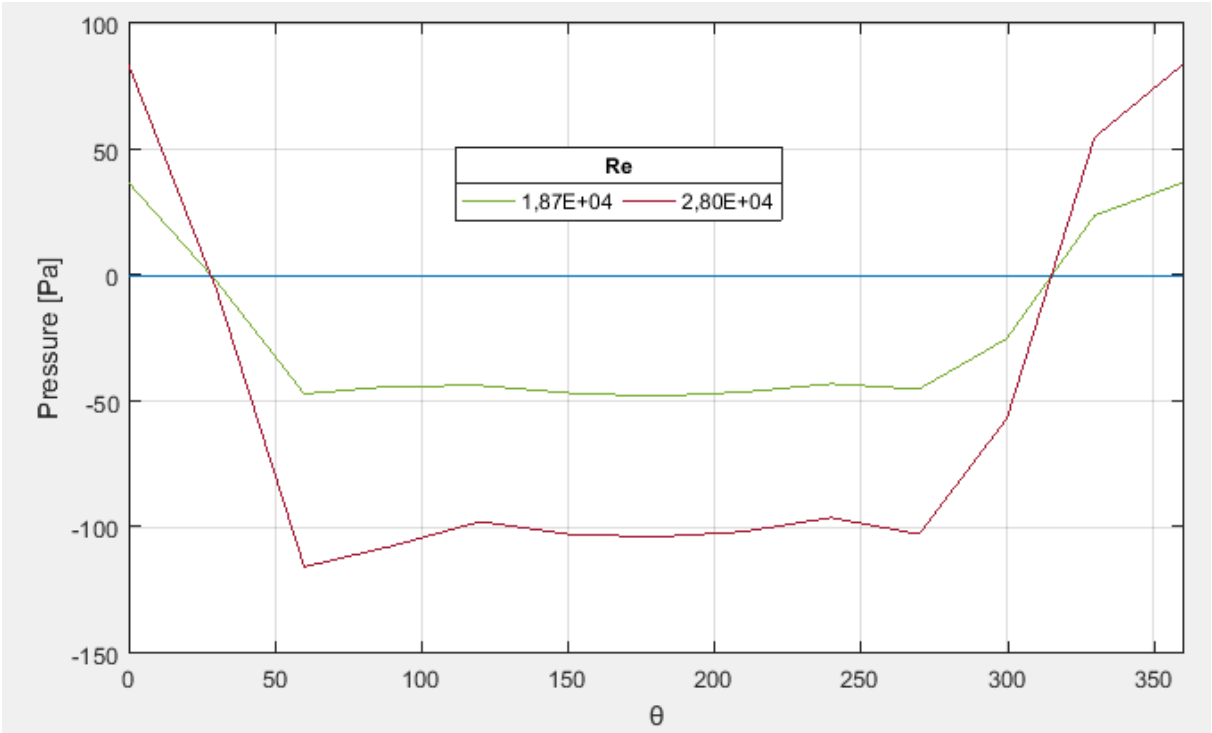

Figure 5.2 Pressure distribution of model P60

Figure 5.3 shows measurements of pressure at the cylinder surface. With the P40 model, in the subcritical range, the location of the separation point was about 80° for a Reynolds number of 1.87x10^4.

It can be clearly seen when flow the flow around the cylinder changes from the subcritical regime to the supercritical regime at a Reynolds number of 2.80x10^4. So the separation point, in this case was located at an angle θ of 120°. This means that the P40 model had already reproduced the supercritical conditions at a wind velocity of about 12 m/s, which is half than in the P140 case and the lowest value of velocity in this study that simulate the supercritical regime conditions

Figure 5.3 Pressure distribution of model P40

5.2 Golf indented pattern

Figure 5.4 shows the distribution of mean surface pressure around de P60 model at Reynolds number of 1,87x10^3 and 2,8x10^4. With the golf model, in the subcritical range, the location of the separation point was about 80° for a Reynolds number of about 1.87x10^4.

However, in the supercritical regimen at a Reynolds number of 2.8x10^4, the separation point moved backward an angle of 120°, and the static pressure on the rear surface came back to its previous position due to the turbulent at the surface. So, this proves that the Golf model was already in the supercritical regime at a wind velocity of about a 12m/s.

Figure 5.4 Pressure distribution of Golf model

5.3   TATARA 1mm indented pattern

Figure 5.3 shows measurements of pressure at the cylinder surface. With the TATARA 1mm model, in the subcritical range, the location of the separation point was about 80° for a Reynolds number of 4.00 x10^4.

It can be clearly seen when flow the flow around the cylinder changes from the subcritical regime to the supercritical regime at a Reynolds number of 4.80x10^4. So the separation point, in this case was located at an angle θ of about 120°. This means that the TATARA 1mm model was simulating the supercritical conditions at a wind velocity of about 24 m/s, which is the highest velocity if the results are compared with the other prototypes in this.
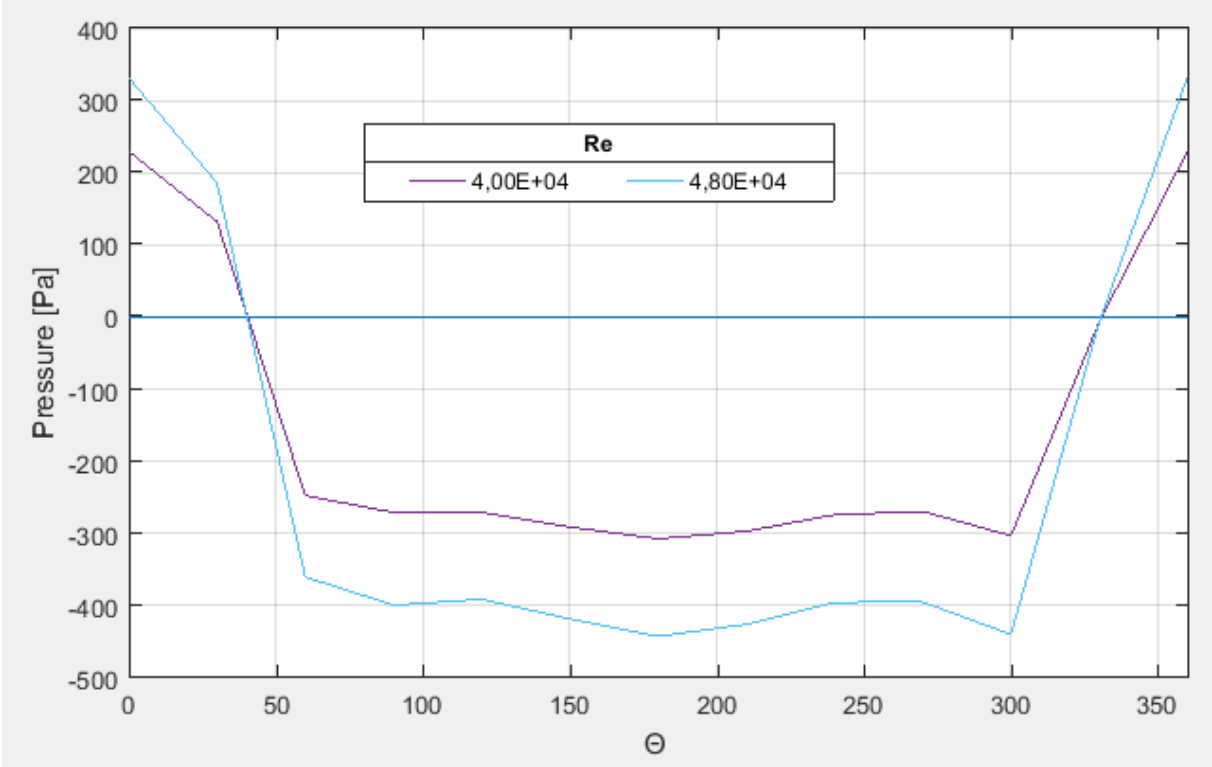
Figure 5.5 Pressure distribution of TATARA 1mm model

6 Conclusion

Experiments carried out in this study on a different roughness surface show that the most appropriate surface to coat the real prototype of the tower of wind turbine is the P60 model as it was demonstrated above. The values of drag coefficient measured as well as the pressure distribution values indicate that with a wind velocity of about 18 m/s the supercritical conditions have already been reproduced. That can be proved because of the separation point and the critical Reynolds number agrees exactly at the same point, as shown in the Figure 4.2 and Figure 5.2.

With the P40 model a lower wind velocity has been approach, although the results obtained in the Drag coefficient test were not totally reliable. The effect obtained by this model, taking in account the roughness coefficient, were not the typical of sandpaper surface. Maybe with a larger range of Reynolds number better results had been obtained.

It was also confirmed that with a dimpled pattern, as shown with the Golf model, better resistance to the wind than with other sandpaper surface or indented patter is provided. Although it was not possible to specify the relationship between the drag coefficient and the Reynolds number.

The results obtained with the TATARA model in the drag coefficient test, Figure 4.4, as well as the pressure test were different than the previous one seen on the literature. It can be based on some difficulties found when testing the model as shown in the Figure B.1.

At the same time, the results derived from the TATARA 1mm model were not satisfactory either. As shown in the Figure 4.4, the drag coefficient follows the same characteristic as the plain cylinder, this may have happened due to the high surface roughness chosen for the TATARA 1mm pattern which has performed in some part of the cylinder as a smooth surface. The results of the pressure distribution shows that the supercritical conditions were not simulated until the velocity of 24 m/s where the separation point reached about 120 °, Figure 5.5.

ANNEXE A

Photos of the prototypes and equipment while the wind tunnel test

Figure A.1 P140 model
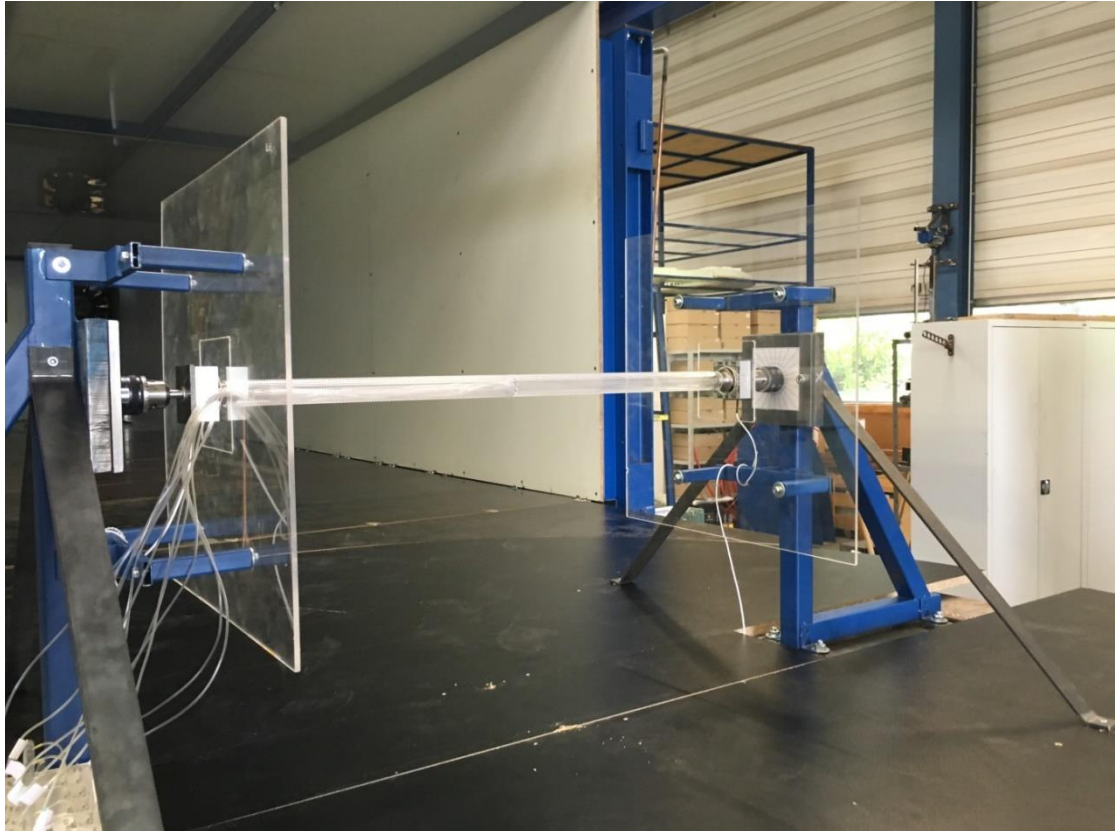

Figure A.2 TATARA model

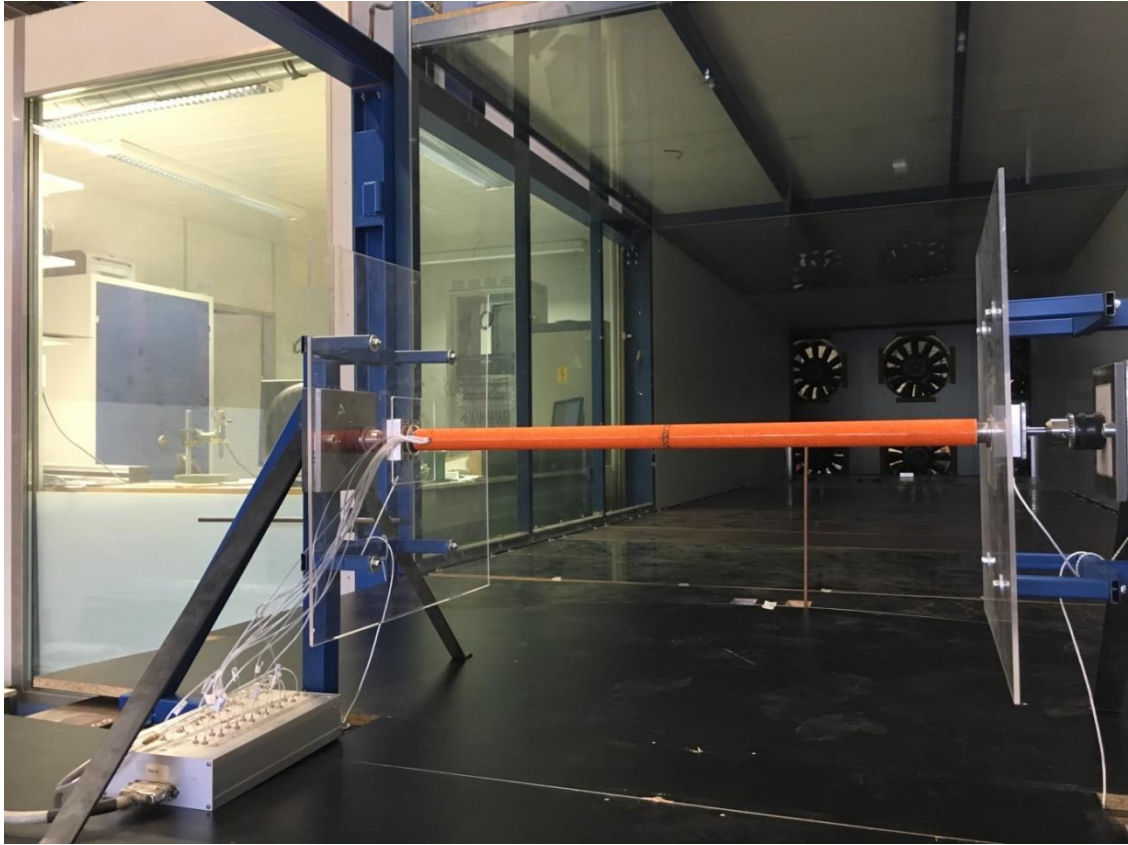**Figure A.3 P60 model**

Figure A.4 Golf model

Figure A.5 P40 model

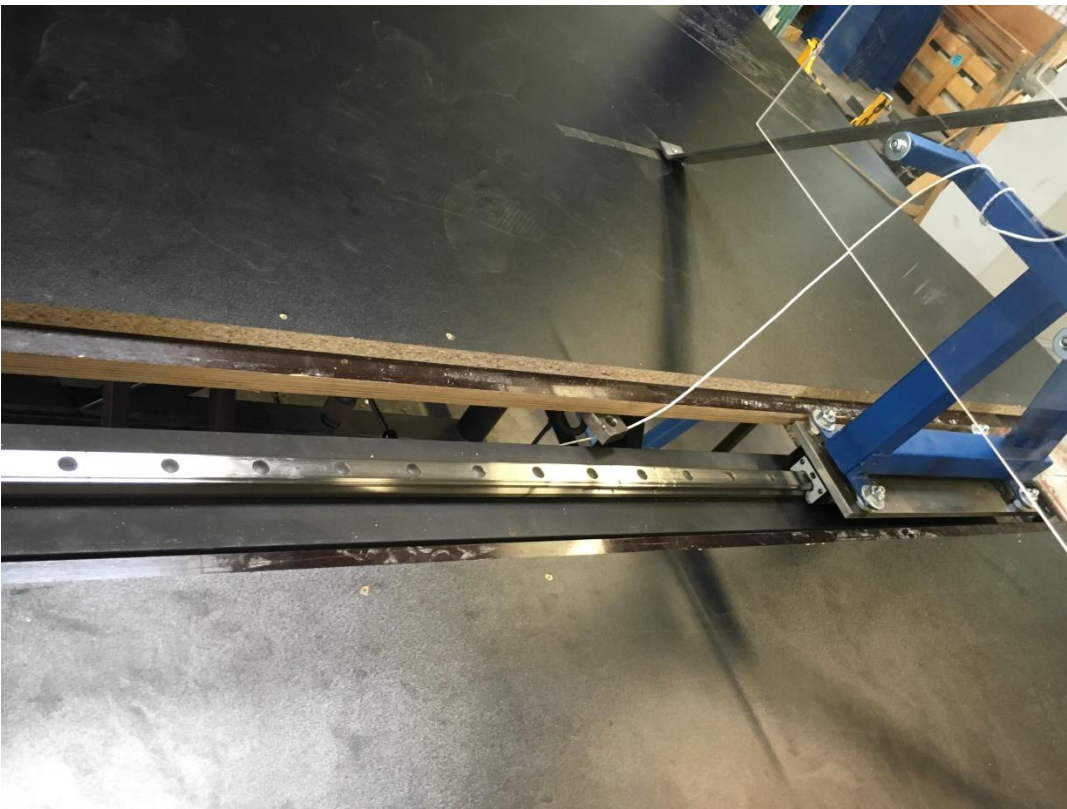**Figure A.6 Plain_3 model**

Figure A.7 TATARA 1mm model

Figure A.8 Guides to move the structure in the rotatory table

Figure A.9 control cubicle
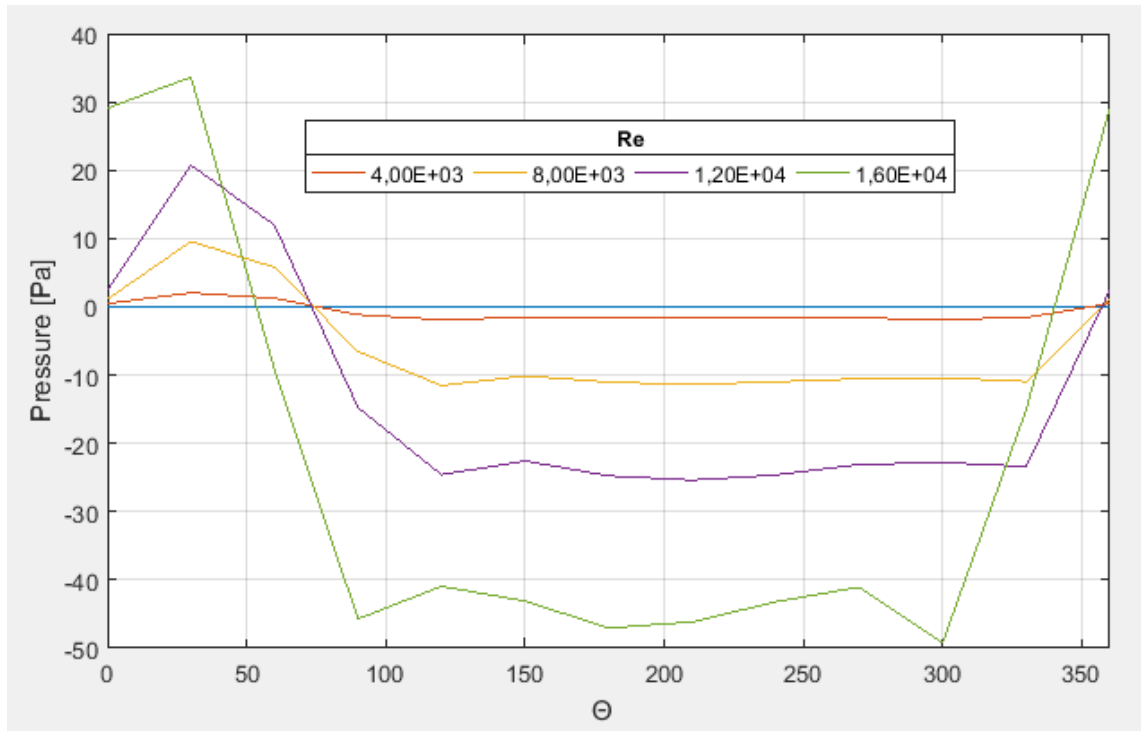
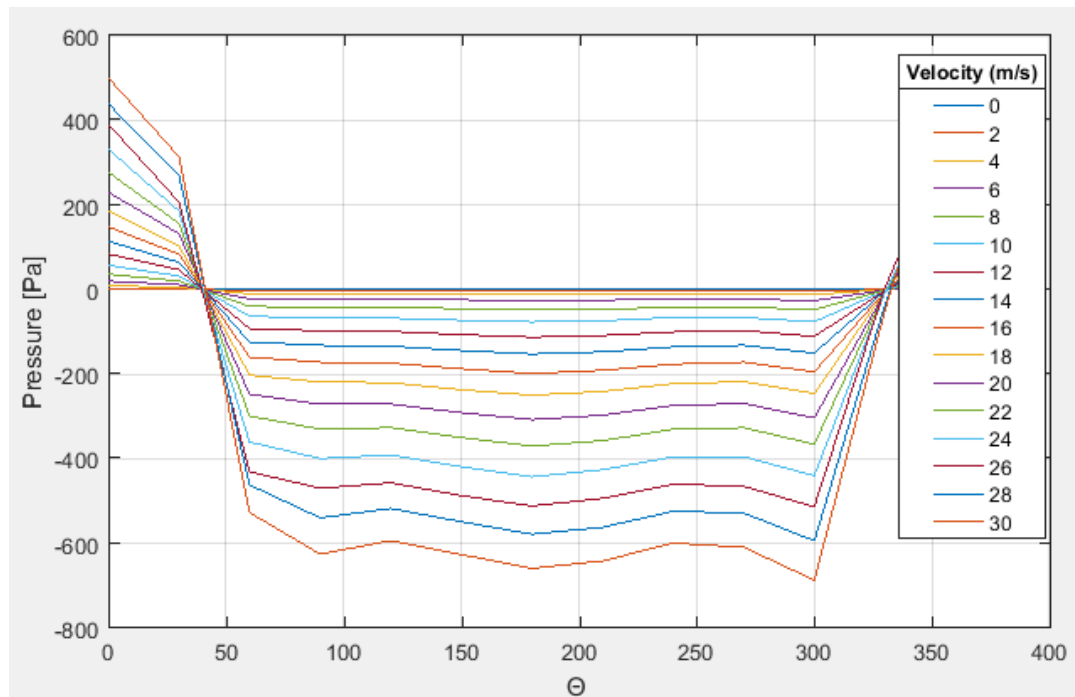Pressure distribution of all the models

Figure B.1 Pressure distribution TATARA model
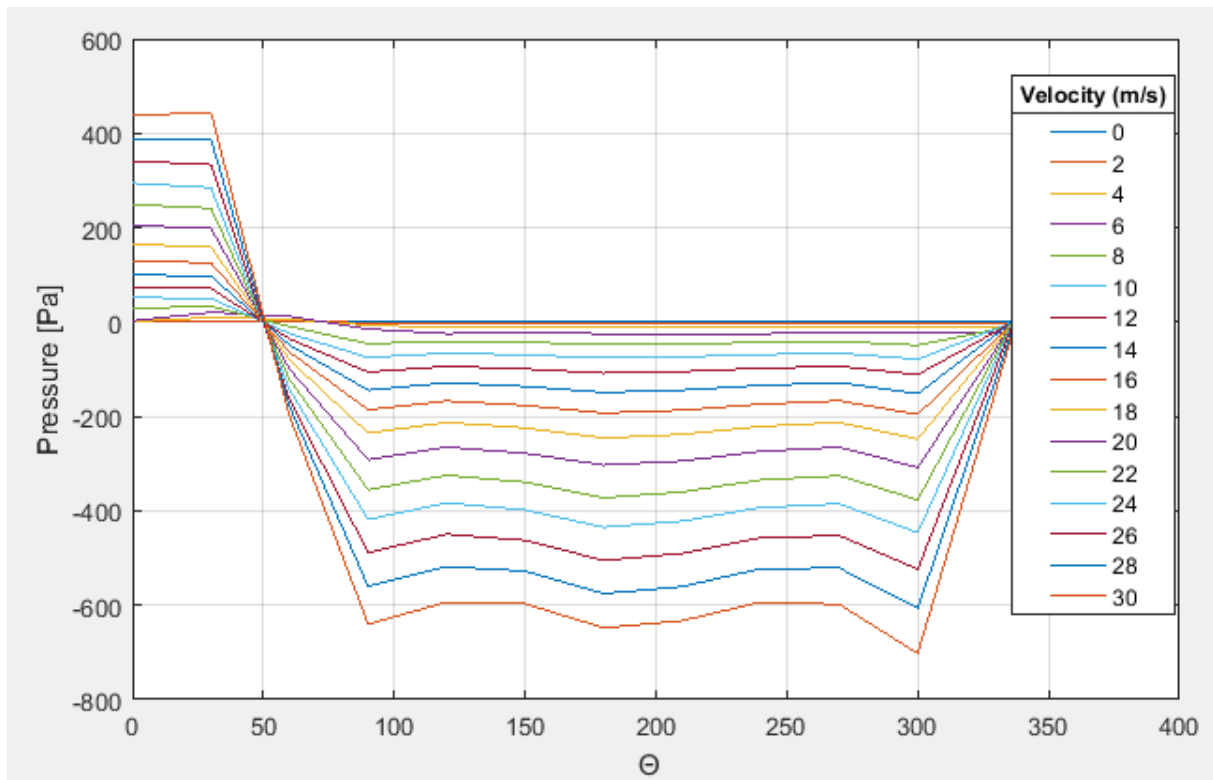

Figure B.2 Pressure distribution of TATARA 1mm model

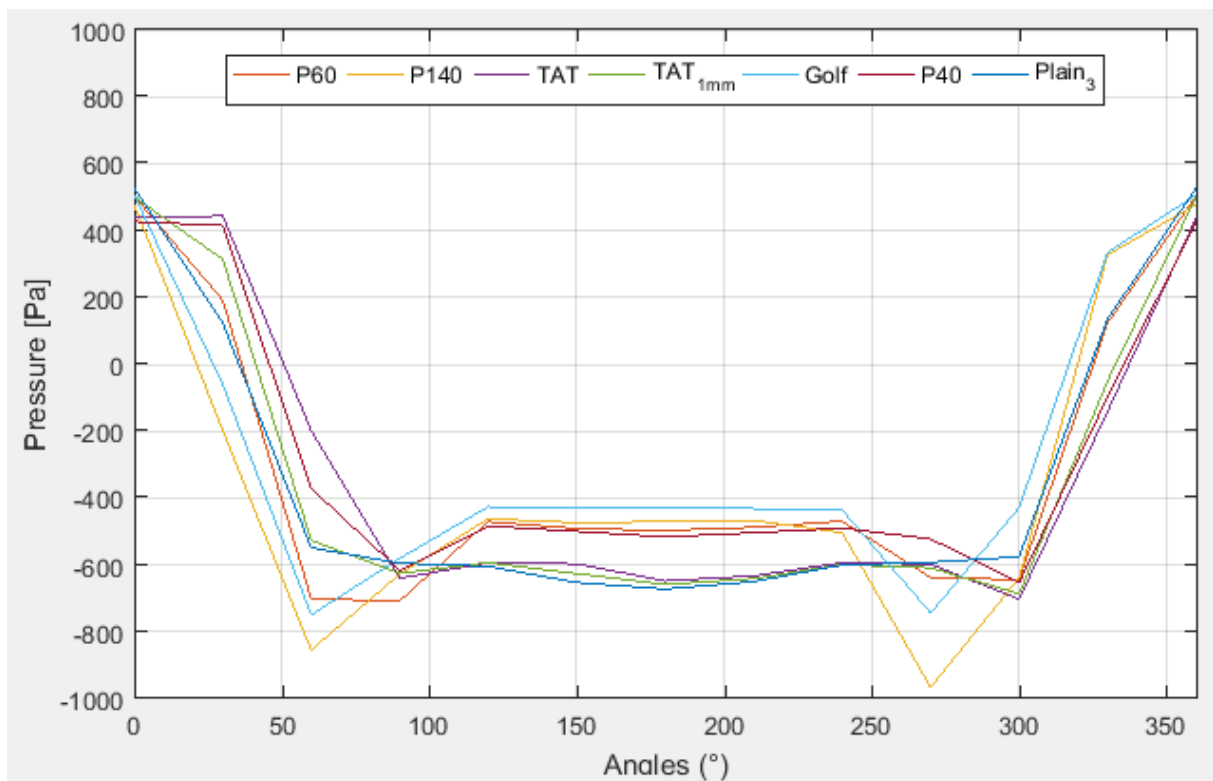**Figure B.3 Pressure distribution of TATARA model**
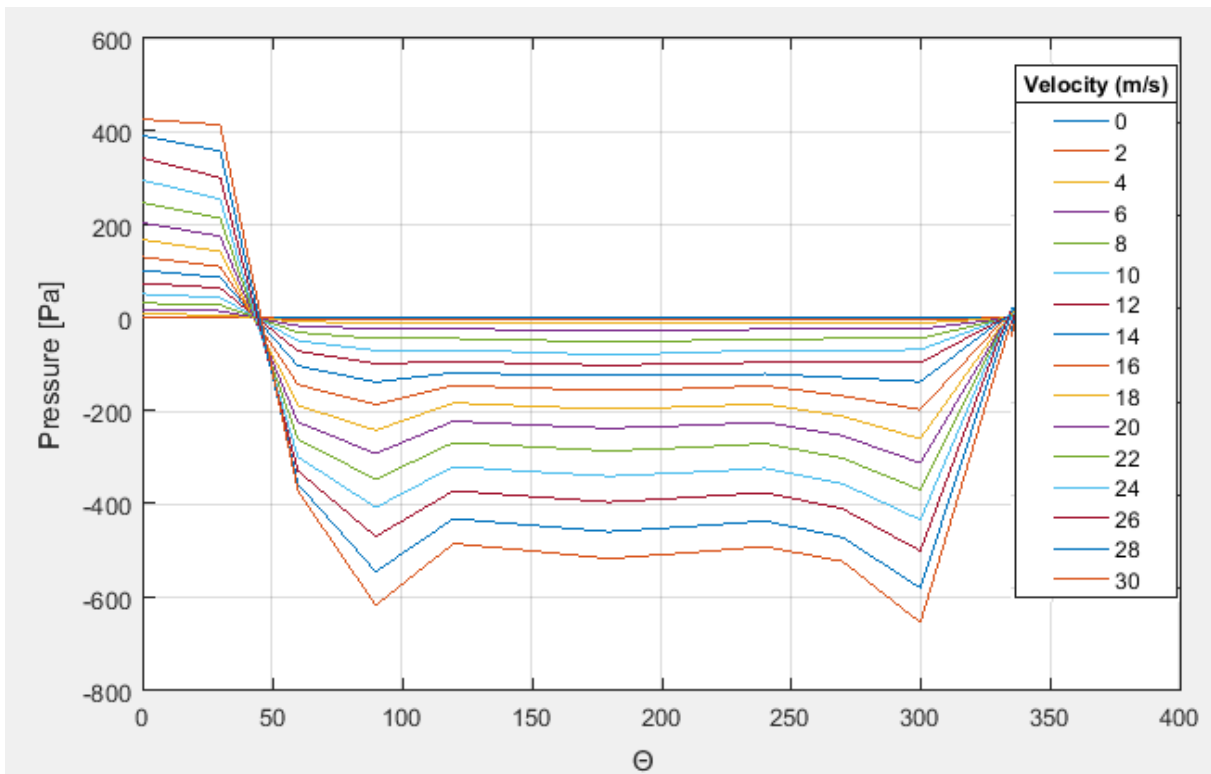

Figure B.4 All pressure distribution
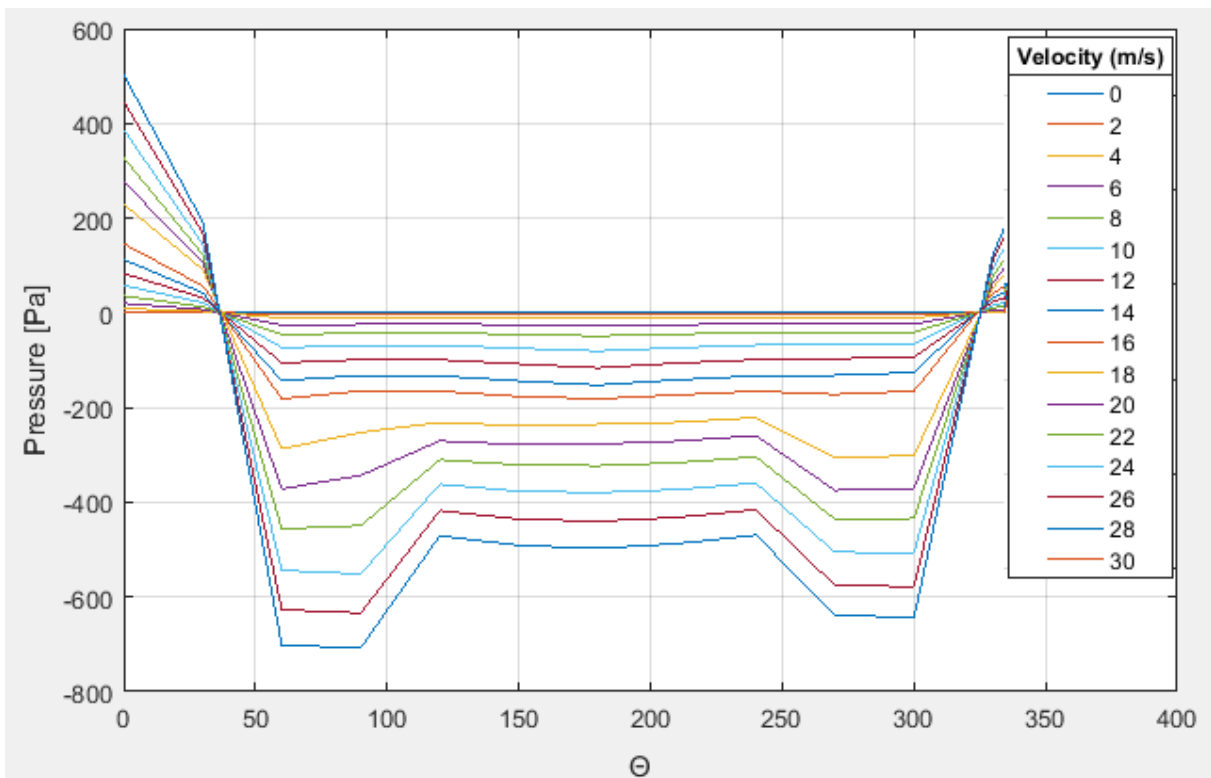
Figure B.5 Pressure distribution of P40 Model

Figure B.6 Pressure distribution of P60 Model
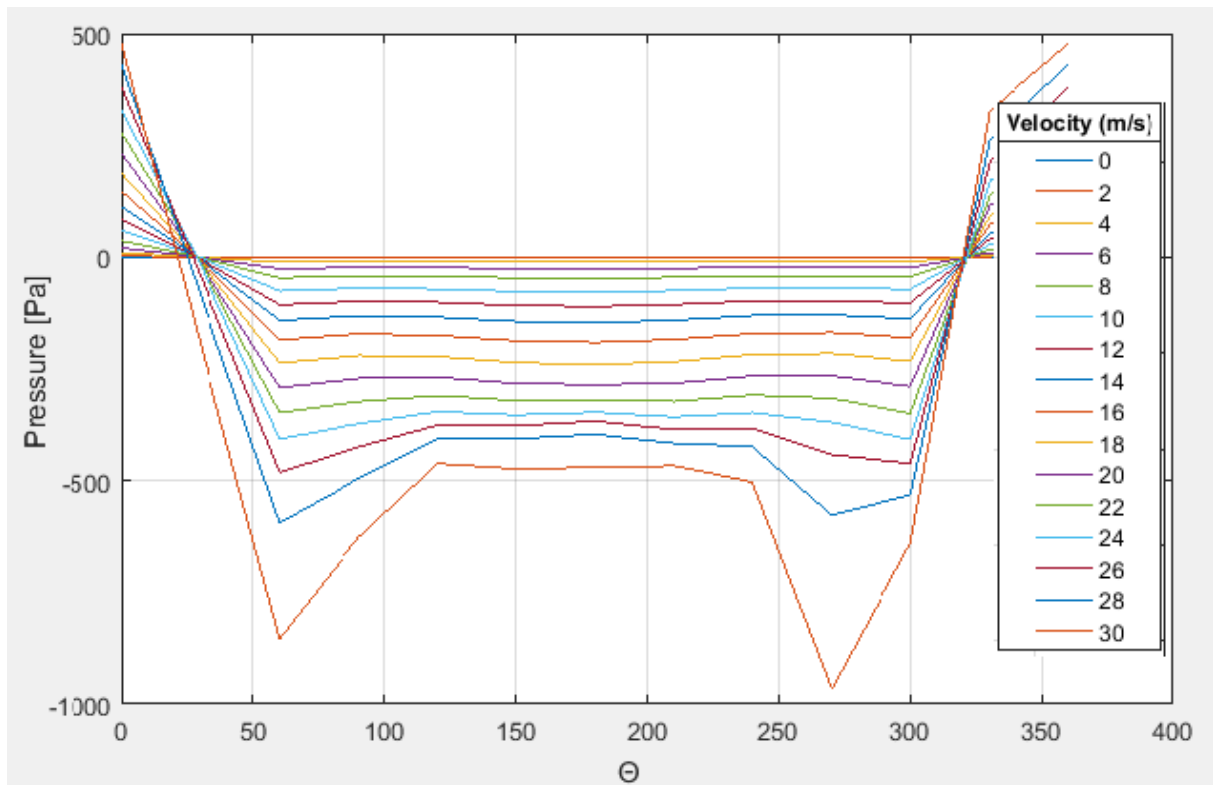
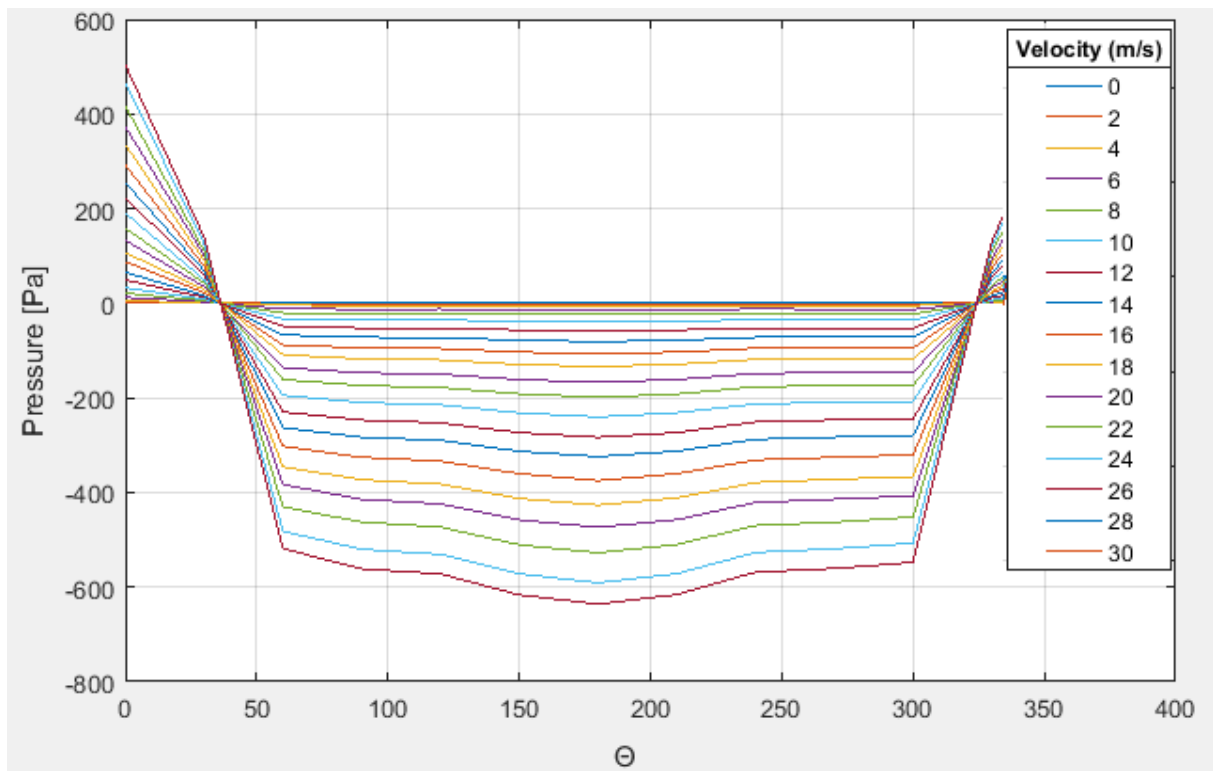**Figure B.7 Pressure distribution of P140 Model**

Figure B.8 Pressure distribution of Plain Model

7   References

[1]   ESDU 81017 1987 Mean forces, pressures and moments for circular cylindrical structures - Finite-length cylinders in uniform and shear flow

[2]   Eurocode 1: „Actions on structures - Part 1-4: General actions Wind actions."

[3]   T. Hojo: "Development of low drag aerodynamically stable cable with indented Processing".

[4]   Miyata, Toshio / Fujiwara, Toru / Yamada, Hitoshi : „Wind-resistant design of cables for the Tatara bridge"

[5]   Hiroshi Katsuchi and Hitoshi Yamada: „Wind-tunnel Study on Dry-galloping of Indented-surface Stay Cable."

[6]   https://en.wikipedia.org/wiki/Vortex_shedding

[7]   https://en.wikipedia.org/wiki/Drag_coefficient

[8]   Sebastian Prokop: „Correct Aerodynamic Scaling of cylindrical Cross-Sections"

[9]   Engineering Sciences Data Unit (ESDU) (1986), "Mean forces, pressures and flow field velocities for circular cylindrical structures: single cylinder with two-dimensional flow", Item Number 80025

[10]   Christian Barré und Guy Barnaud (1995), High Reynolds number simulation techniques and their application to shaped structures model test, Journal of Wind Engineering